Pergamon

Deep-Sea Research II, Vol. 44, No. 9–10, pp. 2049–2083, 1997

Printed in Great Britain

PII: S0967-0645(97)00063-5

0967 0645/98 $19.00 + 0.00

^{234}Th and particle cycling in the central equatorial Pacific

JOHN P. DUNNE,* JAMES W. MURRAY,* JENNIFER YOUNG,* LAURIE S. BALISTRIERI* and JAMES BISHOP†

Abstract—US JGOFS-EqPac ^{234}Th data sets for 1992 boreal spring (Survey I, TT007) and fall (Survey II, TT011) cruises from 12°N to 12°S along 140°W were used to determine rates of ^{234}Th and particle cycling using a thorium sorption model and three coupled particle–thorium models. Sampling methodology had a large impact on model results — estimates of particulate organic carbon varied by a factor of 3 between bottle and in-situ filtration techniques. Adsorption rate constants and residence times from the thorium sorption model showed strong depth, latitudinal and seasonal variability which we were able to attribute to changes in particle concentration. A re-evaluation of the 'particle concentration effect' on the adsorption rate constant, k_1', showed that our values of k_1' increased with particle concentration and were consistent with other study sites with similar particle concentrations. Recycling of particulate organic carbon in the euphotic zone of the central equatorial Pacific was 2–10 times faster than sites previously studied. Calculations of adsorption rate constants from the thorium sorption, coupled particle–^{234}Th and phytoplankton models were extremely dependent on the model treatment of remineralization. Results from the coupled particle–^{234}Th model, where particles have a constant lability, suggested that ^{234}Th recycled three to four times between the dissolved and particulate phases before being removed from the euphotic zone. Aggregation rate constants and sinking rates in the central equatorial system were compared with other sites using the size-fractionated model developed by Clegg and Whitfield (1991, *Deep-Sea Research*, **38**, 91–120). Removal of particles by sinking from the equatorial euphotic zone depended on a mechanism of differential recycling of organic matter in the euphotic zone in which only a fraction of the particles are remineralized and the more refractory particles sink.

INTRODUCTION

Importance of studying particle cycling dynamics

Integrated physical, chemical and biological processes control particle cycling in the upper ocean. The cycle of input of nutrients, production, sinking and remineralization of particles controls oceanic distributions of organic carbon, major nutrients and a suite of trace elements. The equatorial oceans are important places to study these processes because of their large geographical areas and the intensity of particle cycling.

^{234}Th often has been used as an effective tracer of particle cycling to estimate residence times of trace metals and particulate carbon and to calculate the sinking flux of particulate organic carbon (Coale and Bruland, 1985; Murray *et al.*, 1989; Buesseler *et al.*, 1992; Murray *et al.*, 1996). The most basic particle–^{234}Th cycling model is a steady-state mass balance in which the vertical flux of ^{234}Th equals the difference between the rates of in-situ production of ^{234}Th ($t_{1/2} = 24.1$ days) from its long-lived, conservative parent ^{238}U ($t_{1/2} = 4.47 \times 10^9$ years) and in-situ radioactive decay of ^{234}Th. Conversion of the

* School of Oceanography, Box 357940, University of Washington, Seattle, WA, 98195-7940, USA.

† School of Earth and Ocean Sciences, University of Victoria, PO Box 1700 MS 4015, Victoria, BC, Canada.

calculated ^{234}Th flux into a carbon flux requires the organic carbon:^{234}Th ratio of sinking particles. Though this model expresses the bulk removal of ^{234}Th, it does not identify the specific mechanisms of loss. Studying mechanisms of loss using slightly more complex models allows a better understanding of processes controlling particle and trace metal cycling.

Early use of ^{234}Th

One-dimensional scavenging models have been used to characterize the magnitude and variability of ^{234}Th adsorption in the water column and establish potential scavenging mechanisms. Balistrieri *et al.* (1981) used an equilibrium model of metal sorption to particle surfaces to describe mechanisms of removal of a variety of trace metals and to estimate equilibrium constants for metal sorption. Bacon and Anderson (1982) evaluated irreversible and reversible exchange of thorium isotopes between the dissolved phase and bulk particulate material, and were able to isolate reverse (desorption) from forward (adsorption) rates. Coale and Bruland (1985, 1987) and Bruland and Coale (1986) developed a model of upper ocean cycling in which ^{234}Th was used as a tracer of the sinking flux of particulate organic carbon. The mechanism of ^{234}Th scavenging in this model was irreversible and consisted of non-selective adsorption of dissolved ^{234}Th onto sinking particles. They calculated residence times of dissolved ^{234}Th that ranged from 6 to 220 days for a range of ocean environments and found that first-order removal rate constants of particle sinking correlated well with both primary production (Coale and Bruland, 1985) and the sinking flux of particulate organic carbon (Bruland and Coale, 1986).

Attempts have been made to extend the reversible thorium sorption model to regimes with different particle concentrations by incorporating an observed 'particle concentration effect'. Bacon and Anderson (1982) observed a correlation between k_1' and particulate matter. Honeyman *et al.* (1988) also found a good correlation between the log of the adsorption rate constant, k_1', and the log of the particulate mass concentration using a compilation of published data sets that spanned five orders of magnitude of particle concentrations. Brownian pumping was proposed by Honeyman and Santschi (1989) to explain this dependency on particle concentration. They postulated that some dissolved ^{234}Th was actually in a colloidal phase. In their model, colloids coagulate into particles so that particulate ^{234}Th activities result from colloidal coagulation.

Coupled particle–^{234}Th models

The models of thorium adsorption discussed above assume that particles have infinite residence times with respect to remineralization. These models also do not take into account any alterations of particulate matter that occur during coagulation, food web processing or particle sinking. The most direct approach for coupling particle cycling to thorium cycling is to use biological rate parameters to determine a remineralization rate constant. Murnane *et al.* (1990) developed a model to express the coupling between thorium cycling (^{234}Th, ^{230}Th and ^{228}Th) and particle cycling of two particle sizes in the deep ocean and calculated rates of aggregation and disaggregation while assuming no remineralization. Clegg and Whitfield (1990, 1991) developed a similar model to express coupling between ^{234}Th cycling and particle cycling in the surface ocean. In this model, primary production supports a pool of

background suspended matter composed of small, non-sinking particles. These particles aggregate reversibly into large, rapidly sinking particles (Clegg and Whitfield, 1990). Clegg and Whitfield (1991) coupled the ^{234}Th cycle to this particle cycle. They explored spatial variability between the eastern equatorial and sub-arctic Pacific (Clegg and Whitfield, 1991) as well as temporal variability during the JGOFS North Atlantic Bloom Experiment (NABE) (Clegg and Whitfield, 1993). Though Clegg and Whitfield saw large variability in calculated rate constants between sites, they found their model was able to reproduce observed changes in ^{234}Th activities by forcing the model with observed changes in particle cycling. Recently, Murnane *et al.*, 1996 introduced a model that included size fractionation and differentiated between organic particles and inert particles such as clays, opal and carbonate. They then simultaneously evaluated organic carbon and total mass cycling during the NABE.

Oceanographic setting of study area

In this study we explore ^{234}Th as a tracer for particle cycling in the central equatorial Pacific. This region is dominated by upwelling of nutrient-rich water and is characterized as a high nitrate, low chlorophyll (HNLC) environment where high productivity by small phytoplankton is matched by intense grazing and recycling of organic matter predominantly by microzooplankton (Murray *et al.*, 1994; Barber *et al.*, 1996; Landry *et al.*, 1995; Landry *et al.*, 1997). The US JGOFS-EqPac 1992 survey cruises from 12°N to 12°S along 140°W took place during the relatively low nutrient upwelling boreal spring (Survey I) and high nutrient upwelling boreal fall (Survey II) periods of the equatorial seasonal cycle. El Niño conditions were superimposed on this seasonal cycle, which resulted in lower nutrient upwelling conditions relative to climatology (Kessler and McPhaden, 1995). Nevertheless, surface nitrate between 2°N and 7°S latitude was above 2 mM during both cruises. Concentrations at the equator were 3 mM during Survey I and 6 mM during Survey II (Murray *et al.*, 1995). Primary productivity extended below 100 m. The depth of the 0.1% light level was 120 m during both cruises. The integrated production values between 2°N and 2°S were approximately twice as high during Survey II (84–155 mmol C m^{-2} day^{-1}) as Survey I (47–85 mmol C m^{-2} day^{-1}) (Barber *et al.*, 1996). Increases in integrated chlorophyll and particulate carbon from Survey I to Survey II were more modest at 27% and 21%, respectively (Barber *et al.*, 1996; Murray *et al.*, 1996). Phytoplankton growth rates reached values in excess of 1 day^{-1} (Landry *et al.*, 1995). A dynamic steady state for ^{234}Th was illustrated in the constancy of ^{234}Th activities in the EqPac Time Series data of Bacon *et al.* (1996) and in the comparability of the EqPac data sets of Buesseler *et al.* (1995), Bacon *et al.* (1996) and Murray *et al.* (1996).

Objectives of this work

We wish to assess how biological and chemical cycles are coupled in the central equatorial Pacific. Specifically, it is our goal to use the extensive data set of the US JGOFS-EqPac Survey cruises to estimate rate parameters for proposed mechanisms for ^{234}Th and particle cycling. This study of particle–^{234}Th cycling is unique because of the completeness of the complementary data set. As a result, we have been able to make a more extensive evaluation of existing models and arrive at a more realistic evaluation of particle and ^{234}Th cycling in

this region. The objectives are to: (1) review available data from the 1992 US JGOFS-EqPac Survey Cruises, (2) estimate model rate parameters of adsorption, remineralization and aggregation using the EqPac data set and thorium sorption and coupled particle–thorium models, and (3) compare our results with sites previously studied.

MODEL DESCRIPTIONS

In this section we discuss the thorium sorption and coupled particle–thorium models that we used to quantify rates of thorium cycling in the central equatorial Pacific. Four models of increasing complexity are presented in sequence, the first being the thorium sorption model of Bacon and Anderson (1982). We then describe a coupled particle–thorium model in which the particle and ^{234}Th cycles are considered independently assuming a single particle population. As an alternate method of coupling particle and thorium cycling, we introduce a phytoplankton model that distinguishes labile and refractory particle pools. Finally, we discuss aggregation processes between large and small particles in the context of the size-fractionated model of Clegg and Whitfield (1990, 1991, 1993). In this paper we assume steady state and ignore zonal advection (e.g. $u\partial \mathrm{Th_d}/\partial x$) and all diffusion terms (e.g. $\mathrm{d}K_\mathrm{H}/\mathrm{d}x\partial \mathrm{Th_d}/\partial x$, $\mathrm{d}K_\mathrm{H}/\mathrm{d}y\partial \mathrm{Th_d}/\partial y$, $\mathrm{d}K_\mathrm{Z}/\mathrm{d}z\partial \mathrm{Th_d}/\partial z$) while including meridional (e.g. $v\partial \mathrm{Th_d}/\partial y$) and vertical (e.g. $w\partial \mathrm{Th_d}/\partial z$) advective terms. For simplicity, all advection and diffusion terms are omitted in the presentation of continuity equations. For reference, all data parameters are given in Table 1 and all rate parameters in Table 2.

The thorium sorption model is a two-box model of thorium cycling (Fig. 1) in which dissolved ^{234}Th undergoes first-order, reversible adsorption to become particulate ^{234}Th, which sinks through the water column (Bacon and Anderson, 1982). The continuity equations for dissolved and particulate ^{234}Th in this model are:

$$\partial \mathrm{Th_d}/\partial t = \mathrm{U}\cdot\lambda - (\lambda + k_1')\cdot \mathrm{Th_d} + k_{-1}'\cdot \mathrm{Th_p} \tag{1}$$

$$\partial \mathrm{Th_p}/\partial t = k_1'\cdot \mathrm{Th_d} - (\lambda + k_{-1}')\cdot \mathrm{Th_p} - \Psi \tag{2}$$

Table 1. *Summary of data input parameters used for the thorium sorption, coupled particle–thorium and size-fractionated models*

Parameter	Definition	Units	Source
P_r	primary production	mmol C m^{-2} day^{-1}	Barber *et al.*, 1995
P_s	small particles	mmol C m^{-3}	Go-Flo samples (bottles) retained on a GF/F-filter or MULVFS 1–53 μm fraction
P_l	large particles	mmol C m^{-3}	MULVFS > 53 μm fraction
P	total particles	mmol C m^{-3}	$P_\mathrm{s}+P_\mathrm{l}$
F	sinking particle flux	mmol C m^{-2} day^{-1}	^{234}Th model carbon fluxes (Murray *et al.*, 1994)
U	^{238}U	dpm m^{-3}	CTD data: U = 0.0686·Salinity·(1 + σ_Θ/1000)
$\mathrm{Th_d}$	dissolved ^{234}Th	dpm m^{-3}	Go-Flo samples (bottles) passing a 0.4 μm nuclepore filter
$\mathrm{Th_s}$	small particulate ^{234}Th	dpm m^{-3}	Go-Flo samples (bottles) retained on a 0.4 μm nuclepore filter or MULVFS <1–53 μm fraction
$\mathrm{Th_l}$	large particulate ^{234}Th	dpm m^{-3}	MULVFS > 53 μm fraction
$\mathrm{Th_p}$	total particulate ^{234}Th	dpm m^{-3}	$\mathrm{Th_s}+\mathrm{Th_l}$

Table 2. Summary of rate parameters used for the thorium sorption, coupled particle–thorium and size-fractionated models

Parameter	Definition	Units	Associated model, value and source
λ	^{234}Th radioactive decay constant	day^{-1}	All models, $\lambda = 0.02876$ day^{-1}
k_{-1}'	^{234}Th desorption rate constant	day^{-1}	All models, $k_{-1} = 0.0068$ day^{-1}, Clegg and Whitfield (1993)
k_1'	^{234}Th adsorption rate constant	day^{-1}	thorium sorption model, calculated
S	total particle sinking velocity	m day^{-1}	thorium sorption model, calculated
γ	remineralization rate constant	day^{-1}	coupled particle–thorium models, calculated
m_1'	^{234}Th adsorption rate constant	day^{-1}	coupled particle–thorium models, calculated
r_1	aggregation rate constant	day^{-1}	size-fractionated model, calculated
r_{-1}	disaggregation rate constant	day^{-1}	size-fractionated model, $r_{-1} = 5$ day^{-1}, Clegg and Whitfield (1993)
S_l	large particle sinking velocity	m day^{-1}	size-fractionated model, calculated
v	meridional velocity	°lat day^{-1}	MOM output, Chai (1995)
w	vertical velocity	m day^{-1}	MOM output, Chai (1995)

In equations (1) and (2), λ is the decay constant for ^{234}Th ($\lambda = 0.02876$ day^{-1}), k_1' is the adsorption rate constant, k_{-1}' is the desorption rate constant, and Ψ is the removal term for particle sinking. In this model, radioactive decay of ^{238}U (U) supports a pool of dissolved ^{234}Th (Th_d). Th_d adsorbs on particles at a rate of k_1'*Th_d. Particulate ^{234}Th (Th_p) desorbs at a rate of k_{-1}'*Th_p. No distinction is made between small and large particles. Th_d and Th_p are both lost by radioactive decay. The removal flux of ^{234}Th on sinking particles, Ψ, has been defined alternatively as a first-order rate constant for removal of sinking particles multiplied by the particulate ^{234}Th activity (k_2'*Th_p) (Coale and Bruland, 1985) and as gradient in particulate ^{234}Th with depth multiplied by a sinking rate (S*$\partial Th_p/\partial z$) (Bacon and Anderson, 1982), giving:

$$F_{Th} = S \cdot Th_p \tag{3}$$

$$\Psi = k_2' \cdot Th_p = \partial F_{Th}/\partial z = S \cdot \partial Th_p/\partial z + Th_p \cdot \partial S/\partial z \tag{4}$$

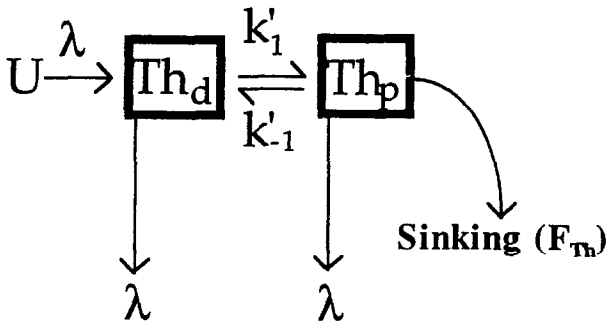

Fig. 1. Flow diagram of the thorium sorption model including reservoirs of dissolved ^{234}Th (Th_d) and particulate ^{234}Th (Th_p) and fluxes of radioactive decay (λ) of ^{234}Th and ^{238}U (U), adsorption (k_1'), desorption (k_{-1}') and sinking (F_{Th}).

where F_{Th} is the sinking flux of ^{234}Th, which equals Th_p multiplied by the sinking rate, S. In order to solve for the rate constants of adsorption, k_1', and removal, k_2', (or k_1' and the sinking rate, S), this model requires data for dissolved ^{234}Th, particulate ^{234}Th and ^{238}U, and requires an assumption of the value of the desorption constant, k_{-1}'. In this study we assumed $k_{-1}' = 0.0068$ day^{-1} from the data compilation of Clegg and Whitfield (1993), which is also consistent with the laboratory experiments of Quigley *et al.* (1996).

This model has the advantage of being conceptually and mathematically simple. In addition, there are many previously published data sets with which to compare results. There are two main disadvantages of this model. First, rate constants predicted by the model are not universal but only apply to specific biological and physical regimes. Second, the model does not include processes that are known to be important in particle cycling such as remineralization and aggregation. If ^{234}Th is to be used to trace particles, the role of these processes must be known.

One reason that rate constants vary from site to site is because they depend on particle concentration. Bacon and Anderson (1982) and Honeyman *et al.* (1988) found support for the following relationship between k_1' and particle concentration:

$$k_1' = k_1 \cdot P^n \tag{5}$$

where P is the particle concentration, n is an observed exponent, and k_1 is an inherent adsorption rate constant independent of particle concentration. Honeyman *et al.* (1988) obtained a value of $n = 0.6$ based on the good correlation ($r^2 = 0.62$) between the log of the adsorption rate constant, k_1', and the log of the particulate mass concentration for published data sets extending over five orders of magnitude of particle concentrations.

We introduce the coupled particle–^{234}Th model in order to describe explicitly both particle and Th cycling (Fig. 2). This model has a particle cycle that includes

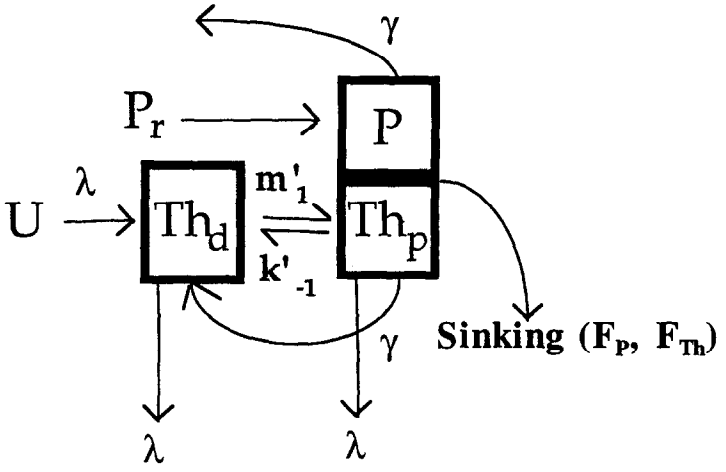

Fig. 2. Flow diagram for the coupled particle–thorium model including reservoirs of particles (P), dissolved ^{234}Th (Th_d) and particulate ^{234}Th (Th_p) and fluxes of primary production (P_r), remineralization (γ), radiocative decay (λ) of ^{234}Th and ^{238}U (U), adsorption (m_1'), desorption (k_{-1}') and sinking of particles (F_P) and ^{234}Th (F_{Th}).

remineralization but does not distinguish between particles of different sizes. By including remineralization, this model takes into account the short residence time of particles in the equatorial euphotic zone. The continuity equations are:

$$\partial P/\partial t = P_r - \gamma \cdot P - \partial F_p/\partial z \tag{6}$$

$$\partial \mathrm{Th_d}/\partial t = \mathrm{U} \cdot \lambda - (\lambda + m_1') \cdot \mathrm{Th_d} + (k_{-1}' + \gamma) \cdot \mathrm{Th_p} \tag{7}$$

$$\partial \mathrm{Th_p}/\partial t = m_1' \cdot \mathrm{Th_d} - (\lambda + k_{-1}' + \gamma) \cdot \mathrm{Th_p} - \partial F_{\mathrm{Th}}/\partial z \tag{8}$$

$$F_p = S \cdot P \tag{9}$$

$$F_{\mathrm{Th}} = S \cdot \mathrm{Th_p} \tag{10}$$

where U, $\mathrm{Th_d}$, $\mathrm{Th_p}$, k_{-1}' and λ are defined as before. This model requires additional data on primary production (P_r), the total particle concentration (P), and the settling flux of particles (F_p). Solution of the particle equation gives the remineralization rate constant (γ), which is the same for both particles and ^{234}Th. The removal term ($\partial F_{\mathrm{Th}}/\partial z$) is identical in the thorium sorption and coupled particle–^{234}Th models. Though k_1' and m_1' are both adsorption rate constants, they do not have the same meaning. Solving equations (1) and (7) for m_1' gives the relationship between these two estimates of the adsorption rate constant as:

$$k_1' = m_1' - \gamma \cdot \mathrm{Th_p}/\mathrm{Th_d} \tag{11}$$

In the thorium sorption model, loss terms from the particulate ^{234}Th pool include desorption, decay and sinking. In the coupled particle–thorium model, an additional loss term for remineralization of particulate ^{234}Th is included to account for recycling of particles. Equation (11) shows that m_1' reflects gross or true adsorption while k_1' reflects true adsorption minus remineralization. The coupled particle–^{234}Th model has the advantage of explicitly including information on particle recycling but has the same disadvantage as the previous models of not differentiating between particles of different reactivity or size.

If the particle pool is composed of particles with different reactivities, then the coupled particle–thorium model may overestimate the remineralization of particulate ^{234}Th and thus over-estimate the adsorption rate constant, m_1'. To accommodate this possibility, we extended the coupled particle–thorium model by explicitly dividing the total particulate concentration into two compartments: a labile phytoplankton pool and a refractory pool of heterotrophs and detritus. We call this alternative coupled model the phytoplankton model (Fig. 3). While Murnane *et al.* (1996) invoked differing labilities to distinguish between organic and inorganic particles, we invoke the phytoplankton model to distinguish between reactive and refractory organic particles. The continuity equations for this model are:

$$\partial P_{\mathrm{phy}}/\partial t = P_r - (\gamma/f + r_1) \cdot P_{\mathrm{phy}} \tag{12}$$

$$\partial P/\partial t = r_1 \cdot P_{\mathrm{phy}} - \partial F_p/\partial z \tag{13}$$

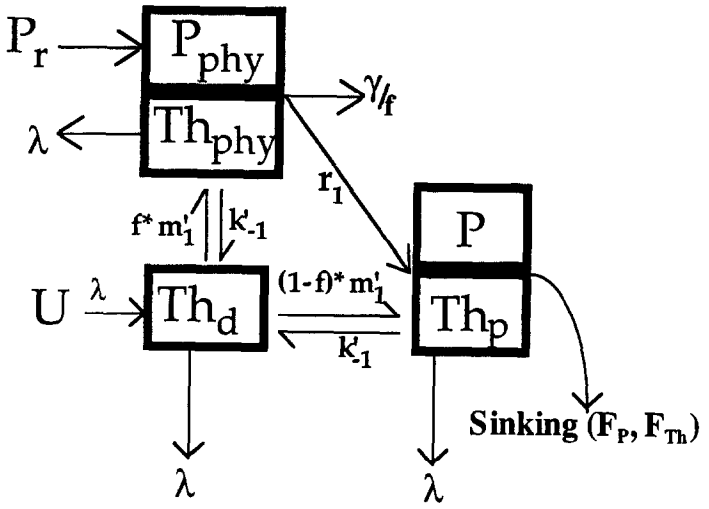

Fig. 3. Flow diagram for the phytoplankton model including the fraction of total particles that is phytoplankton (f), reservoirs of phytoplankton (P_{phy}), refractory particles (P), dissolved ^{234}Th (Th_d) and particulate ^{234}Th (Th_p) and fluxes of primary production (P_r), remineralization (γ), ^{234}Th and ^{238}U (U) radiocative decay (λ), adsorption (m_1'), desorption (k_{-1}') and sinking of particles (F_p) and ^{234}Th (F_{Th}).

$$\partial Th_d/\partial t = U \cdot \lambda - (\lambda + m_1') \cdot Th_d + (k_{-1}' + \gamma/f) \cdot Th_{phy} + k_{-1}' \cdot Th_p \tag{14}$$

$$\partial Th_{phy}/\partial t = m_1' \cdot f \cdot Th_d - (\lambda + k_{-1}' + \gamma/f + r_1) \cdot Th_{phy} \tag{15}$$

$$\partial Th_p/\partial t = m_1' \cdot (1-f) \cdot Th_d + r_1 \cdot Th_{phy} - (\lambda + k_{-1}') \cdot Th_p - \partial F_{Th}/\partial z \tag{16}$$

$$F_p = P \cdot S \tag{17}$$

$$F_{Th} = Th_p \cdot S \tag{18}$$

where P_r, γ, F, U, Th_d, k_{-1}' and λ are defined as before. This model differentiates between labile, phytoplankton carbon (P_{phy}) and refractory carbon (P). It also includes ^{234}Th associated with phytoplankton carbon (Th_{phy}) and refractory carbon (Th_p). f is the fraction of total particulate organic carbon ($P_{phy} + P$) that is in the labile, phytoplankton pool (P_{phy}). In this model, there is first-order, reversible adsorption of ^{234}Th onto both particle pools but only the phytoplankton pool can remineralize.

In an attempt to model aggregation and sinking of particles in the surface ocean, Clegg and Whitfield (1990, 1991a) developed a size-fractionated model of coupled particle–thorium cycling (Fig. 4). This model assumes first-order aggregation, disaggregation and remineralization between large (P_l) and small (P_s) particle pools. Small particles are assumed to be non-sinking while large particles rapidly sink with a settling rate, S. The ^{234}Th cycle is superimposed on the particle cycle by first-order, reversible adsorption onto small particles only. The model is defined by the equations of state for two particle pools (small particles, P_s, and large particles, P_l) and three ^{234}Th pools (dissolved ^{234}Th, Th_d, small

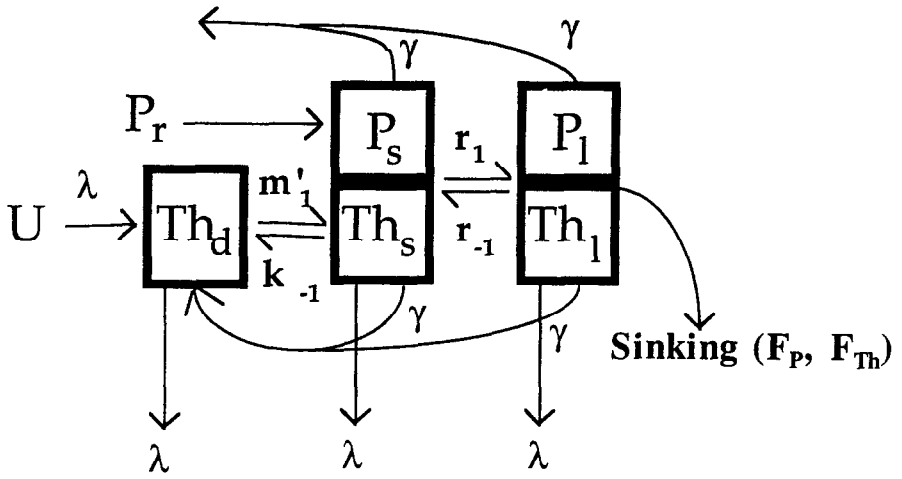

Fig. 4. Flow diagram for the size-fractionated model including reservoirs of small particles (P_s), large particles (P_l), dissolved ^{234}Th (Th_d), small particulate ^{234}Th (Th_s) and large particulate ^{234}Th (Th_l) and fluxes of primary production (P_r), remineralization (γ), aggregation (r_1), disaggregation (r_{-1}), ^{234}Th and ^{238}U (U) radiocative decay (λ), adsorption (m_1'), desorption (k_{-1}') and sinking of particles (F_l) and ^{234}Th (F_{Th}).

particulate ^{234}Th, Th_s, and large particulate ^{234}Th, Th_l) (equations 19–25). Th_d is the same as in the previous models, but P and Th_p in the previous models are equal to $P_s + P_l$ and $Th_s + Th_l$, respectively, in the size-fractionated model. This model requires the same data inputs as for the simple coupled model plus additional values for large particle concentrations and large particulate ^{234}Th activities. The continuity equations for the size-fractionated model are:

$$\partial P_s/\partial t = P_r - (\gamma + r_1) \cdot P_s + r_{-1} \cdot P_l \tag{19}$$

$$\partial P_l/\partial t = r_1 \cdot P_s - (\gamma + r_{-1}) \cdot P_l - \partial F_p/\partial z \tag{20}$$

$$\partial Th_d/\partial t = U \cdot \lambda - (\lambda + m_1') \cdot Th_d + (k_{-1}' + \gamma) \cdot Th_s + \gamma \cdot Th_l \tag{21}$$

$$\partial Th_s/\partial t = m_1' \cdot Th_d + r_{-1} \cdot Th_l - (\lambda + k_{-1}' + \gamma + r_1) \cdot Th_s \tag{22}$$

$$\partial Th_l/\partial t = r_1 \cdot Th_s - (r_{-1} + \lambda + \gamma) \cdot Th_l - \partial F_{Th}/\partial z \tag{23}$$

$$F_p = P_l \cdot S_l \tag{24}$$

$$F_{Th} = Th_l \cdot S_l \tag{25}$$

In the size-fractionated model primary production, P_r, supports a pool of small particulate matter, P_s, that aggregates at a rate of $r_1 * P_s$ into large particulate matter, P_l. Both small and large particles remineralize with a rate constant γ identical to γ in the coupled particle–^{234}Th model. Large particles disaggregate at a rate of $r_{-1} * P_l$ or sink as flux at a rate of $\partial F_p/\partial z$ with a sinking rate of S_l.

In the ^{234}Th component of the model, radioactive decay of ^{238}U supports a pool of dissolved ^{234}Th or Th_d. Th_d adsorbs onto small particles at a rate of m_1'*Th_d. ^{234}Th desorbs from small particles at a rate of k_1'*Th_s. Small particulate thorium, Th_s, aggregates along with the small particles into the large particulate fraction at a rate of r_1*Th_s. Large particulate ^{234}Th, Th_l, disaggregates back to the small particulate fraction at a rate of r_{-1}*Th_l and sinks at a rate of $\partial F_{Th}/\partial z$ with a sinking velocity S_l. Both Th_s and Th_l remineralize with a rate constant γ back to Th_d. γ is the same for particles and ^{234}Th. Th_d, Th_s and Th_l are all subject to loss by radioactive decay. The adsorption rate constants in the coupled particle–^{234}Th model and the size-fractionated model, both defined here as m_1', are nearly identical. The constant in the size-fractionated model is slightly lower because Th_s is slightly smaller than Th_p. The advantage of this model over the coupled particle–^{234}Th model is in differentiating suspended from sinking particles.

AVAILABLE DATA

In this section we present the input data from the JGOFS EqPac Survey Cruises for the thorium and particle models (Table 1). Though most previous studies have described the particle cycle in terms of total mass, we have used organic carbon because our ultimate goal is to use ^{234}Th cycling to trace carbon cycling in the upper ocean. We include particle calculations based on total mass, however, for ease of comparison with previous studies at other sites. We concentrate our interpretation on EqPac Survey II because the data are more complete.

^{238}U activity was calculated from salinity (S) and potential density (σ_Θ) using the data sets of Ku *et al.* (1977) and Chen *et al.* (1986) to obtain the regression: $U = 0.0686 \cdot S \cdot (1 + \sigma_\Theta/1000)$.

Dissolved and small particulate ^{234}Th were measured using the operational definition of a 0.4 μm Nuclepore filter (Fig. 5(a) and (b)). These samples were obtained by whole bottle filtration of 30 l Go-Flo bottles. We assume that sampling bottles do not catch the large particulate fraction, so that the >0.4 μm data reflects the composition of small particles (Bishop and Edmond, 1976). We also collected unfiltered, or total ^{234}Th samples, which are presented in Murray *et al.* (1996). When comparing our total ^{234}Th data with dissolved and particulate data from the same station and depth, we found the sum of the dissolved plus particulate ^{234}Th to be systematically 13% ($\pm$13%) lower than the total ^{234}Th data. Because we do not know the source of the discrepancy, we have chosen to use the dissolved and particulate data without additional correction. Variability in the dissolved ^{234}Th data prevented the accurate calculation of horizontal and vertical gradients. Gradients in dissolved ^{234}Th were estimated by multiplying the observed gradients in total ^{234}Th from Murray *et al.* (1996) by the observed ratio of dissolved to total ^{234}Th (0.71 ± 0.14). During Survey II we also collected particulate data using the Multiple Unit Large Volume Filtration System (MULVFS) (Bishop *et al.*, 1985) (Fig. 5(b)). The MULVFS was configured with two sequential 1.0 μm quartz filters behind a 53 μm pre-filter for the 1–53 μm fraction. MULVFS 1–53 μm particulate ^{234}Th data were systematically 100 dpm m^{-3} higher than the whole-bottle filtration (0.4 μm) data (an average of 38% higher). The origin of these discrepancies is not clear. We use each of the small particulate ^{234}Th data types without modification to calculate 'bottle' and 'MULVFS' estimates of rate parameters.

We also have two available data sets for the concentration of organic carbon in small

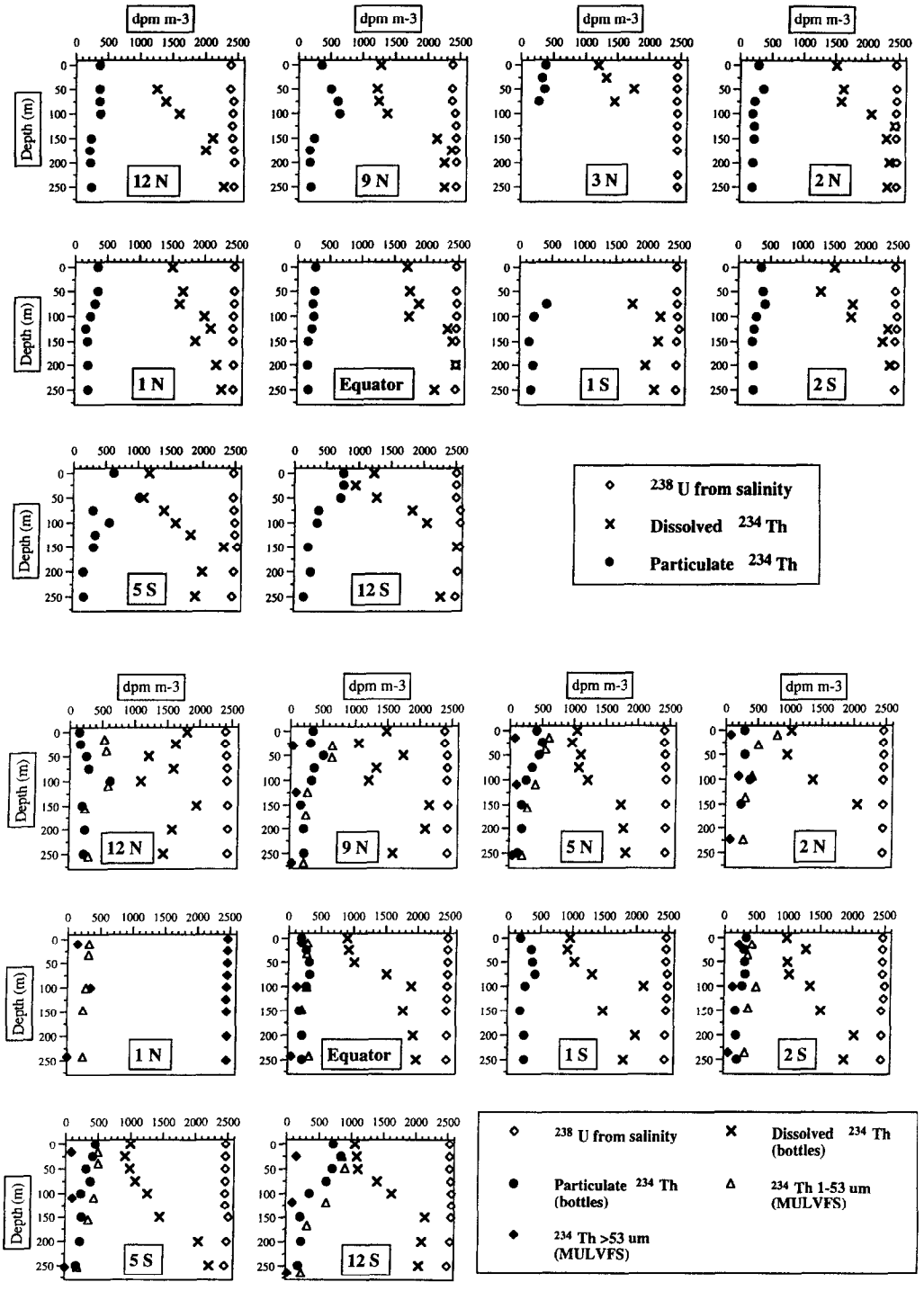

Fig. 5. ^{234}Th dissolved and particulate data from 0.4 μm Nuclepore filtration from Go-Flo bottles for Survey I (a) and Survey II (b). (b) includes particulate data for MULVFS 1–53 μm and > 53 μm fractions for Survey II. Units are dpm m^{-3}.

suspended particles: those collected using 10 l Niskin or 30 l Go-Flo bottles, and those from MULVFS. The bottle samples were obtained by filtration using glass fiber filters (GF/F) with a nominal pore size of 0.6 μm. The sampling and analytical procedures including blank values were presented in Murray *et al.* (1996). Carbon and ^{234}Th analysis were performed on the same bottle casts only during Survey II. Total mass also was determined on MULVFS samples. The bottle and MULVFS sampling methods for organic carbon produced widely different results. The GF/F bottle data are 3.2 ± 1.4 times higher than the MULVFS 1–53 μm fraction. This is opposite to the trend observed between the bottle and MULVFS 1–53 μm particulate ^{234}Th data.

The origin of the difference between organic carbon data collected by bottles versus in-situ filtration techniques is unresolved. The regression for organic carbon versus beam attenuation shows much more scatter for bottles ($r^2 = 0.69$) than for MULVFS ($r^2 = 0.94$) data (Bishop, in press). Similar differences between in-situ filtration and bottles have been observed elsewhere (Altabet *et al.*, 1992). The disparity between these methods may be partly due to the presence of a relatively large population of sub-micron phytoplankton and bacteria (Kirchman *et al.*, 1995; Chung *et al.*, 1996; Barber *et al.*, 1996). As >80% of the phytoplankton population was smaller than 1.0 μm, the 1.0 μm quartz filters MULVFS system may not have collected a significant fraction of biomass. During EqPac Time Series II, Bacon *et al.* (1996) used an in-situ pumping system similar to MULVFS, except that they used a GF/F filter behind a single 1.0 μm quartz fiber filter. In the upper 100 m the Bacon *et al.* (1996) quartz fiber filter caught, on average, 1.3 mmol C m^{-3}. Their GF/F filter caught, on average, 0.67 mmol C m^{-3}, or 48% of the value from the quartz filter. In comparison, the second MULVFS quartz filter only caught, on average, 30% of the first MULVFS quartz fiber filter. Together, both MULVFS quartz filters amount to only 0.85 mmol C m^{-3} at the equator during Survey II or 43% of the total value of 2.0 mmol C m^{-3} observed by Bacon *et al.* (1996). This comparison between in-situ pumping systems suggests that the MULVFS 1–53 μm concentrations in the upper 100 m should be increased by a factor of 1.12–2.32 for comparison with bottle data. For the small particulate concentration, P_s, we have used parallel estimates from bottle GF/F data and the MULVFS 1–53 μm data interpolated to depths at which we have bottle ^{234}Th. We utilize these two estimates to calculate upper and lower estimates of the model rate constants.

For the large particulate concentration, P_l, we used the >53 μm mass and carbon data from MULVFS. During Survey II we analyzed sub-samples of the MULVFS >53 μm size fractions for ^{234}Th to obtain estimates for Th_l (Fig. 5(b)). The shallowest two MULVFS samples at each station were collected at depths that ranged from 9 to 40 m and 93 to 124 m, respectively. For each station we have interpolated the MULVFS data points between 0 and 300 m to depths at which total, dissolved and particulate and trap measurements of ^{234}Th were taken. The concentration (and ^{234}Th activity) of large particles is set equal to zero at the sea surface (a zero flux boundary condition) consistent with the characteristic low atmospheric deposition in this region (Duce and Tindale, 1991).

Primary production data are from Barber *et al.* (1996), interpolated to depths at which ^{234}Th measurements were conducted. Basing the particle cycle on carbon has the advantage of removing the uncertainty associated with assuming the carbon to mass ratio for the particles produced in primary production. Where necessary, however, we convert from organic carbon to mass using a mass:organic C ratio of 3.04 determined from the MULVFS 1–53 μm data from the upper 100 m. Flux estimates for carbon (F_p) were obtained from the

total ^{234}Th mass balance model from the ^{234}Th flux estimates of Murray *et al.* (1996) calculated from the deficiency of ^{234}Th relative to ^{238}U, incorporating vertical and meridional advective fluxes from observed gradients in ^{234}Th multiplied by advection velocities from Chai (1995). These ^{234}Th fluxes were converted to organic carbon fluxes using the organic carbon to ^{234}Th ratio from drifting sediment traps of PIT design. The flux of carbon used here was thus obtained, not independently from ^{234}Th, but as an output of the total ^{234}Th mass balance model. The trap and model fluxes are similar; however, over both cruises and for all depths trap fluxes averaged $13 \pm 63\%$ higher than model fluxes. The data set can be viewed and downloaded from the web-site for the US-JGOFS data system (http://www1.whoi.edu/jgofs.html). Ranges given here are total ranges. Error and variability estimates are given as $\pm$ one standard deviation. Probability (P) results are given for the two-tailed test. Error analysis of the input data used here is given in Murray *et al.* (1996).

DISCUSSION

Thorium sorption model

The thorium sorption model is relatively simple and allows the widest comparison with previous studies. We use this model to calculate an adsorption rate constant, the average sinking rate of particulate material, the residence times of dissolved ^{234}Th relative to adsorption (the inverse of the adsorption rate constant), and the residence time of particulate ^{234}Th with respect to removal. We also present a re-evaluation of the 'particle concentration effect' on the adsorption rate constant.

Adsorption rate constant, k_1' and sinking rates, S. The adsorption rate constant, k_1', is calculated from the dissolved ^{234}Th mass balance equation. Solution of equation (1) for k_1', assuming steady state and ignoring zonal advection and horizontal and vertical diffusion, gives:

$$k_1' = \frac{\left(\lambda \cdot (\mathrm{U} - \mathrm{Th_d}) + k_{-1}' \cdot \mathrm{Th_p} - v\frac{\partial \mathrm{Th_d}}{\partial y} - w\frac{\partial \mathrm{Th_d}}{\partial z}\right)}{\mathrm{Th_d}} \tag{26}$$

where v and w are the meridional and vertical velocities, respectively. Advection terms generally had very little effect on the value of k_1', with the exception of the estimates at 75 and 100 m near the equator. The percentage change in k_1' between 5°N and 5°S due to the incorporation of advection terms (Fig. 6) averaged $\pm 11\%$. Adsorption rate constant estimates using bottle $\mathrm{Th_p}$ are shown for three depth intervals (0–75 m, 100–150 m and 200–250 m) as a function of latitude for Survey II in Fig. 7(a)–(c). The least-squares propagated error for individual values of k_1' averaged 17%, while total variability at each latitude within each depth bin averaged 32%. The magnitude of k_1' decreased significantly ($P < 0.001$ using the Mann–Whitney U-test; Sokal and Rohlf, 1995; Rohlf and Sokal, 1995) from 0.038 ± 0.014 to 0.019 ± 0.010 day^{-1} between 0 and 75 m (Fig. 7(a)) and between 100 and 150 m (Fig. 7(b)). The decrease was also significant ($P < 0.02$) from 100 to 150 m to 0.0099 ± 0.0046 between 200 and 50 m (Fig. 7(c)). These decreases are concomitant with significant decreases ($P < 0.001$ in both cases) in particulate organic carbon, consistent with the previously observed correlation between k_1' and particle concentration (Bacon and Anderson, 1982; Honeyman *et al.*, 1988). The values of k_1' showed a significant decrease

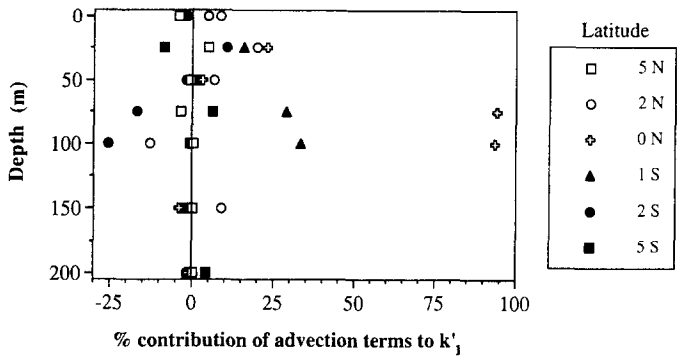

Fig. 6. The percent effect of advection on the adsorption rate constant (k_1', day^{-1}) from the thorium sorption model versus depth for all stations 5°N to 5°S during Survey II.

with depth at all stations except 9°N and 12°N ($P<0.05$ using product-moment correlation; Sokal and Rohlf, 1995; Rohlf and Sokal, 1995). There was also a significant polewardly-negative meridional decrease in particulate organic carbon from MULVFS ($P<0.05$) and bottles ($P<0.01$) away from the equator in the shallowest depth interval (Fig. 7(a)). Consistent with the correlation between k_1' and particle concentration, k_1' showed a similar polewardly negative decrease ($P<0.01$).

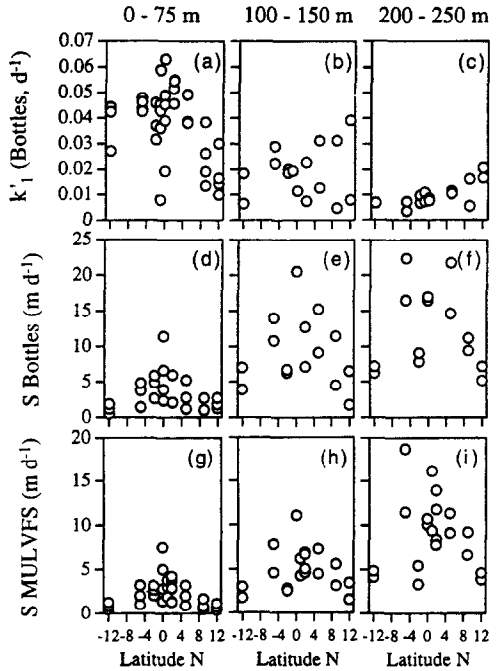

Fig. 7. Average adsorption rate constants, k_1' (day^{-1}), using bottle data (Fig. 6(a)–(c)) and sinking rates, S (m day^{-1}), using bottle (Fig. 6(d)–(f)) and MULVFS (Fig. 6(g)–(i)) data from the thorium sorption model. Values are plotted for Survey II versus latitude for the 0–75, 100–150 and 200–250 m depth ranges.

Estimates of k_1' using bottle and MULVFS Th_p data agreed, on average, within 4%. This good agreement is because the fraction of ^{234}Th in the particulate phase in the surface layers was small (10–40%). The value of k_1' was determined by the magnitude of Th_d as the desorption term (k_{-1}*Th_p) was small relative to the deficiency term. Values of k_1' were sensitive, however, to the value of Th_d.

Sinking velocities (S) are shown for three depth intervals (0–75 m, 100–150 m and 200–250 m) as a function of latitude for Survey II using bottle particulate ^{234}Th data in Fig. 7(d)–(f) and MULVFS particulate ^{234}Th data in Fig. 7(g)–(i). S was obtained by dividing the ^{234}Th flux, obtained from the advection-corrected ^{234}Th deficiency (e.g. F_{Th}, Murray *et al.*, 1996) by the particulate ^{234}Th activity at that depth ($S = F_{Th}/Th_p$). The depth and meridional trends in sinking rate were similar, regardless of whether Th_p was taken from bottles (Fig. 7(d)–(f)) or MULVFS (Fig. 7(g)–(i)). The least-squares propagated error for S from bottles and MULVFS averaged 23%, while variability at each latitude within each depth bin averaged 36%. The magnitude of S from bottles increased significantly ($P < 0.001$) from 3.3 ± 2.5 m day^{-1} between 0 and 75 m (Fig. 7(d)) to 9.2 ± 5.0 m day^{-1} between 100 and 150 m (Fig. 7(e)). The increase was not significant ($P > 0.1$) from 100 to 150 m to 12.3 ± 5.8 m between 200 and 250 m (Fig. 7(f)). The magnitude of S from MULVFS increased significantly ($P < 0.001$) from 2.2 ± 1.6 m day^{-1} between 0 and 75 m (Fig. 7(g)) to 4.9 ± 2.4 m day^{-1} between 100 and 150 m (Fig. 7(h)). The increase was also significant ($P < 0.001$) from 100 to 150 m to 9.1 ± 4.2 m day^{-1} between 200 and 250 m (Fig. 7(i)). The strong increase in the sinking rates with depth was heavily dependent on the estimate of F_{Th}. As the radioactive deficiency was generally confined above 150 m, the error on F_{Th} (and thus on the sinking rate) increased rapidly with depth (Murray *et al.*, 1996). Both bottle and MULVFS estimates of S (Fig. 7(d)–(i)) showed significant meridional decreases away from the equator ($P < 0.05$).

The sinking rates estimated here are lower than those typically reported for sinking material (for example, Diercks and Asper, 1997) because this model does not distinguish between sinking and non-sinking particles. The sinking rate in this model is an average for the entire particle population. For a heterogeneous particle pool, changes in the observed value of S can occur either because of an increase in the sinking rate of particles which actually sink or by an increase in the fraction of the particle population that sinks. These two possibilities cannot be distinguished using this model.

Th residence times with respect to scavenging. In order to compare our results of ^{234}Th cycling with previous studies in this region, we calculated residence times of dissolved ^{234}Th with respect to adsorption and particulate ^{234}Th with respect to removal by sinking. Our average results for the upper 75 m are compared with those of Bruland and Coale (1986) from the MC-80 cruise in the boreal fall of 1980 along 160°W (Fig. 8). This cruise took place during mild El Niño, moderate cold tongue conditions (Climate Prediction Center data archive). Their residence times were calculated using a single surface water value of dissolved and particulate ^{234}Th. For this comparison alone we assumed that desorption is negligible ($k_{-1}' = 0$) to be consistent with the calculations of Bruland and Coale (1986).

The residence time of dissolved ^{234}Th with respect to adsorption (τ_d) is simply the inverse of k_1' (equation (11)). τ_d had a maximum value of 90 days at the equator during Survey I and decreased to 30–50 days at higher latitudes. During Survey II, τ_d was relatively constant at 30 days except for a steady increase to 70 days at 12°N. The values

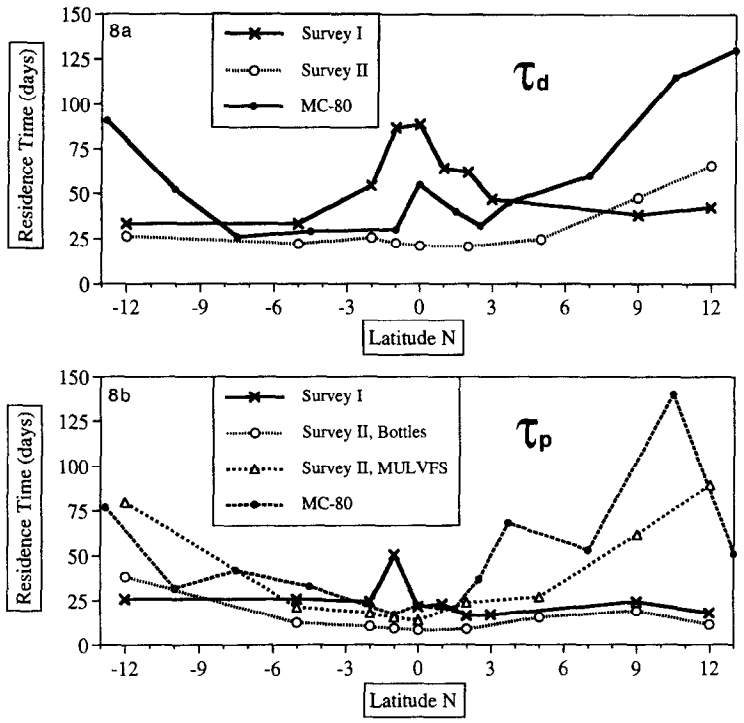

Fig. 8. Residence times (days) of dissolved ^{234}Th with respect to net adsorption (a) and particulate ^{234}Th residence times with respect to scavenging (b) from the MC-80 cruise (Bruland and Coale, 1986), Survey I and Survey II.

from the MC-80 cruise showed long residence times north of 5°N, similar to Survey II, and a small maximum at the equator similar to Survey I. The values from the MC-80 cruise differed in magnitude in both cases. The relatively large values of τ_d at the equator during Survey I are consistent with the extensive biological recycling observed during the El Niño conditions of Survey I and Time Series I cruises (Murray *et al.*, 1994; Landry *et al.*, 1995). Development of the coupled particle–^{234}Th model is necessary to explicitly incorporate changes in food web structure.

The residence time of particulate ^{234}Th with respect to removal (τ_p) is simply the inverse of the removal rate constant, k_2' (equation 4). Like τ_d, τ_p had a maximum of 50 days at the equator during Survey I and decreased to 15–25 days at higher latitudes. τ_p during Survey II, on the other hand, had a broad minimum at the equator at about 10 days using the bottle data for Th_p. τ_p calculated for Survey II using the MULVFS data and from the MC-80 data increased to values higher than 50 days at high northern and southern latitudes. Similarly, values calculated using MULVFS data and from MC-80 also had an equatorial minimum and increased to higher values (> 50 days) at higher latitudes. The variation in the residence time of particulate ^{234}Th with respect to removal during Survey I at the equator may be due to relatively efficient particle recycling near the equator which is consistent with meridional changes in the *f*-ratio (the fraction of total production supported by nitrate) given in Murray *et al.* (1996). The shorter particle residence times observed during Survey II are consistent with a shift in food web structure during the cold

tongue conditions to include more large diatoms and decreased percent grazing by microzooplankton (Landry *et al.*, 1995).

These values of the residence times of ^{234}Th with respect to adsorption and removal are quite long relative to coastal locations with high particulate concentrations. There values can be less than one day (values of $\log(k_1') > 0$). These values are also long relative to the movement of water in this region. For example, a typical value of meridional advection of 0.4 m s^{-1} in the upper 75 m implies that a water parcel at the equator can move one degree of latitude in 3 days. The timescales of adsorption and removal in this model suggest that advection may play a significant role in the mass balances of dissolved and particulate thorium in spite of the observations discussed earlier that advection terms generally make only a small contribution to k_1'. This issue is addressed elsewhere (Dunne and Murray, submitted).

Comparison of adsorption rate constant, k_1', with particle concentration. Using previously published data, we calculated values of the adsorption rate constant, k_1', for a wide range of oceanographic conditions. Values range from about $\log k_1' = 0.5$ to $\log k_1' = -4$. Particle concentration (P) appears to be a major factor controlling much of this variability. The first attempt to conceptually and mathematically link the ^{234}Th cycle to the particle cycle was through the 'particle concentration effect' of Honeyman *et al.* (1988). They plotted $\log k_1'$ versus $\log P$ for all available data and found the linear correlation with a slope of 0.6 (equation 5). We present a revised version of the $\log k_1'$–$\log P$ relationship in Fig. 9. Included are values of k_1' calculated using the ocean water column data sets summarized by Honeyman *et al.* (1988). In addition, we included values of k_1' calculated using more recent data from Coale and Bruland (1985), Murray *et al.* (1989), Wei and Murray (1991, 1992), Baskaran *et al.* (1992), Buesseler *et al.* (1992), Moran and Buesseler (1993), Buesseler *et al.* (1995), Bacon *et al.* (1996) and Liang *et al.* (submitted). We have omitted the data set of Cochran *et al.* (1986) for interstitial pore waters as these conditions do not necessarily reflect ^{234}Th cycling in an open water environment.

Data sets for Survey I and Survey II using MULVFS particle mass and particulate ^{234}Th are consistent with all other estimates at similar particle concentrations and show a highly significant correlation between $\log k_1'$ and $\log P$. This revised figure is different from that of Honeyman *et al.* (1988) in that k_1' increases with increasing particle concentration until particle concentrations (P) of 300 mg m^{-3} and is then constant at $P > 300$ mg m^{-3}. This compilation suggests that the adsorption reaction is zero order with respect to particle concentration at concentrations greater than 300 mg m^{-3}. This result would be consistent with the Brownian Pumping model of Honeyman and Santschi (1989) if: (1) the rate of Th_p production is limited by coagulation rates as opposed to adsorption rates, and (2) coagulation rate constants in high particle regimes do not exceed $\log(0.5) = 3$ day^{-1}. The regression between the log of the particle concentration and the log of the adsorption rate constant is discussed further in our comparison between the thorium sorption and coupled particle–thorium models.

Coupled particle–^{234}Th model

The thorium sorption model is limited because it does not allow remineralization of the particles onto which ^{234}Th adsorbs. Thus, the value calculated for k_1' is a measure of 'net' adsorption (true adsorption minus remineralization (equation 11)). It is necessary to utilize

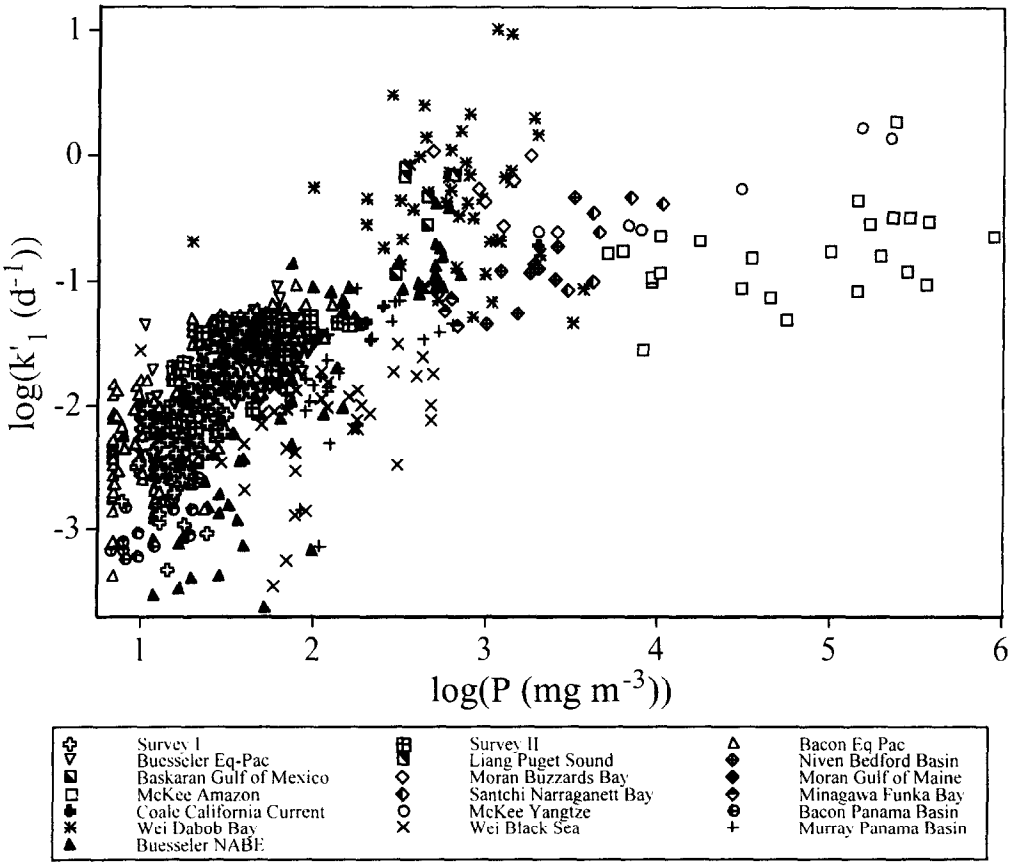

Fig. 9. Correlation between log particle concentration (log(mg m^{-3})) and log adsorption constant constant (log(day^{-1})) using the thorium sorption model. Values are plotted for Survey I, Survey II and using data from 14 other published studies.

the coupled particle–^{234}Th model to explicitly solve the model for remineralization and distinguish 'total' from 'net' adsorption. Using the coupled particle–^{234}Th model, we calculate the remineralization rate constant of particles and particulate thorium and, from it, an adsorption rate constant that is free from the influence of remineralization. We then revisit the question of how the adsorption rate constant relates to particle concentration. Sinking velocities (S) and particulate residence times with respect to removal (τ_p) from the coupled particle–^{234}Th model are numerically identical to those from the thorium sorption model.

Remineralization rate constant. We calculate the average remineralization rate constant, γ, in the 0–100 m depth interval, by rearranging equation (6):

$$\gamma = \frac{\left(\int_0^{100} Pr\, dz - F_{100}\right)}{\int_0^{100} P\, dz} \tag{27}$$

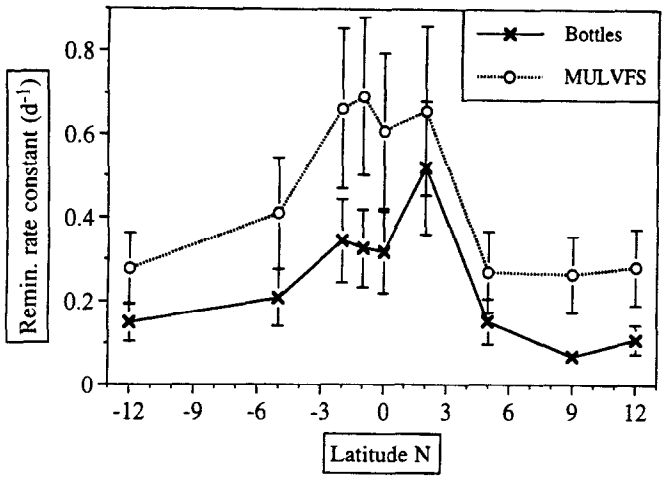

Fig. 10. Average remineralization rate constants (day^{-1}) based on carbon from bottles and MULVFS data from the coupled particle–thorium model. Values are plotted for Survey II versus latitude for the 0–100 m depth range.

where P_r is primary production, F_{100} is the sinking flux of carbon at 100 m and P is the particle concentration expressed in terms of carbon. The meridional variations of the average remineralization rate constant, γ, in the surface layer for Survey II (0–100 m) are shown in Fig. 10 for both bottle and MULVFS particle concentration data sets. The average values of γ from both data sets showed pronounced maxima about the equator. As the integrated particle concentrations from bottles did not have a strong latitudinal trend and the sinking flux of particulate organic carbon was consistently low (Murray *et al.*, 1996), variability in the value of γ using bottle data mostly reflected changes in primary production. Integrated particle concentrations in the upper 100 m from bottles were 2.2 times higher than those from MULVFS samples between 2°N and 2°S and 1.8 times higher than those from MULVFS off the equator (3°–12°N, S). This led to values of γ from bottle data (0.08–0.51 day^{-1}) that were much lower than values calculated using the MULVFS data (0.27–0.70 day^{-1}). Remineralization rate constants estimated from bottle samples at the equator are comparable to estimates by Walsh *et al.* (1995) made during the time-series cruises using changes in the integrated particle load (IPL) measured by mass-calibrated beam attenuation.

Below the euphotic zone γ can only be directly calculated from the gradient in the sinking particle flux with depth. Unfortunately, the percentage decrease in the ^{234}Th calibrated sediment trap flux from 120 m to 250 m was statistically insignificant (Murray *et al.*, 1996), thus prohibiting direct calculation of γ. Previous analysis of depth profiles of particle flux have utilized both power functions consistent with shallow remineralization and exponential functions consistent with deep remineralization (Martin *et al.*, 1987; Pace *et al.*, 1987; Najjar *et al.*, 1992). As the remineralization rate constant below the euphotic zone is small, but positive, it is necessary to assign a value. Here we assign values described by a smooth function. Particle fluxes from a five-year time series at station ALOHA showed an average decrease of 20% in the 100–250 m

depth interval (Karl *et al.*, 1996). We chose an exponentially decreasing function for γ of the form:

$$\gamma_{>100} = \frac{(\gamma_{0-100} \cdot n \cdot z_{100})}{(1 - e^{(-n \cdot z_{100})})} \cdot e^{(-n \cdot z_{100})} \tag{28}$$

where γ_{0-100} is the value of between 0 and 100 m, $z_{100} = 100$ m and n was adjusted to a value of 0.02 m^{-1} to simulate a 20% decrease in flux between 100 m and 250 m. Values of γ for 125–250 m ($\gamma_{>100}$) ranged from 0.01 to 0.06 day^{-1} using this function.

Comparison with other studies shows that these are reasonable estimates. Comparison between the sinking flux of particulate organic carbon at 120 m (Murray *et al.*, 1996) and moored trap flux measurements at depths of 1166 ± 164 m (Honjo *et al.*, 1995) gives $\gamma = 0.005 \pm 0.003$, assuming a linear decrease in flux, and $\gamma = 0.009 \pm 0.006$, assuming an exponential decrease in flux. Emerson *et al.* (1995) made mass balances for oxygen, nitrogen and argon at the Hawaii Ocean Time Series (HOT) site. Combining their oxygen respiration rates with suspended particulate organic carbon data from bottles (Tupas *et al.*, 1995) gives $\gamma = 0.02$–0.04 between 100 and 175 m. Williams and Purdie (1991) measured oxygen consumption in seawater incubations giving $\gamma = 0.37$ at 120 m and $\gamma = 0.02$–0.08 between 150 and 250 m at the HOT site. Jenkins (1987) used tritium, helium and oxygen mass balances in the North Atlantic gyre to calculate oxygen utilization rates. Combining these data with suspended particulate organic carbon data from bottles from the Bermuda Atlantic Time Series (Knap *et al.*, 1994) gives $\gamma = 0.032$ at 111 m to $\gamma = 0.023$ below (138–392 m). All estimates assume a stoichiometry of $O_2/C = 1.4$ (Laws, 1991; Williams and Robertson, 1991). Bacon *et al.* (1996) found that approximately 30% of the carbon sinking past 120 m remineralized by 200 m during the EqPac Time Series Cruises at the equator, 140°W. This corresponds to a value of γ of 0.02 day^{-1}, which compares well to our parameterization of 0.03 day^{-1} in this same depth interval.

Adsorption rate constant, m_1'. With these estimates of γ, the adsorption rate constant, m_1', of the coupled particle–^{234}Th model can be calculated from equation (7) (including meridional and vertical advection) as:

$$m_1' = \frac{\left(\gamma \cdot (U - Th_d) + (\gamma + k_{-1}') \cdot Th_p - v\frac{\partial Th_d}{\partial y} - w\frac{\partial Th_d}{\partial z}\right)}{Th_d} \tag{29}$$

Results for m_1' averaged over the 0–75 m depth interval for Survey II are shown in Fig. 11. The estimates above 100 m increased dramatically in accordance with equation (11): adsorption constants from the coupled particle–^{234}Th model (m_1') were 3.2 ± 1.1 times higher than those from the thorium sorption model (k_1') using bottle γ and Th_p values and 6.8 ± 1.5 times higher using MULVFS γ and Th_p values. Accordingly, meridional and vertical advection terms had a much smaller effect on m_1' (averaging (3%) than on k_1' (averaging (11%). High values of both γ and Th_p in the MULVFS data served to increase the value of m_1' over that from the bottle data. The trend toward higher values south of the equator seen for k_1' (Fig. 7(a)) was also seen for m_1' using this model (Fig. 11). The adsorption rate constants (m_1') below 100 m were increased very little by the incorporation of remineralization as remineralization rate constants in this depth region have been specified as relatively low. Below 100 m, adsorption constants from the coupled particle–^{234}Th model (m_1') are an average of 7% higher than those from the thorium

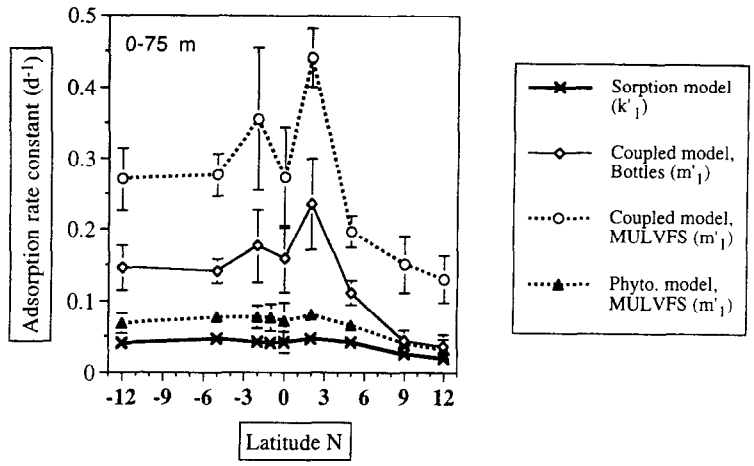

Fig. 11. Average adsorption rate constants (day^{-1}) based on carbon data using the thorium sorption model, the coupled particle–thorium model and the phytoplankton model. Values are plotted for Survey II versus latitude for the 0–75 m depth range.The values are plotted as a function of latitude and were calculated using both bottle and MULVFS particulate data. Values for k_1' calculated from the thorium sorption model described earlier are also plotted for comparison.

sorption model (k_1') using bottle γ and Th_p values and an average of 30% higher using MULVFS γ and Th_p values.

Both log m_1' and log k_1' have a significant linear correlation with log P (Fig. 12). The slope of the log m_1'–log P relationship for the coupled particle–^{234}Th model (slope = 2.0 from either bottles or MULVFS values of m_1') is much higher than that observed for the thorium sorption model (slope = 0.88) or that observed by Honeyman *et al.* (1988) (slope = 0.6). There are many potential explanations for this larger dependency on particle concentration.

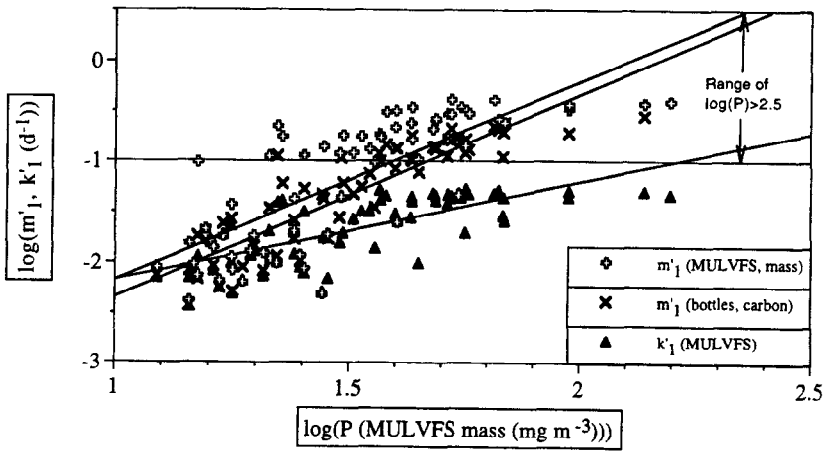

Fig. 12. Correlation between log particle concentration (log(mg m^{-3})) and log adsorption constant constant (log(day^{-1})) using the thorium sorption model and coupled particle–thorium model (bottles and MULVFS). Values are plotted for Survey II.

Comparison with the data of Bacon *et al.* (1996), discussed earlier, suggests that a small part (perhaps 20%) of this dependency may be an artifact of the fact that the MULVFS 1–53 μm mass data underestimates particulate mass at high particle concentrations. This steeper slope (2.0) may be a real chemical phenomenon, suggesting that the reaction order of adsorption is indeed greater than one with respect to particle concentration. This hypothesis is consistent with the presence of highly adsorptive phytoplankton exudates in the surface layers observed by Niven *et al.* (1995), which may be absent in the deeper layers or perhaps due to the temperature dependence of the adsorption reaction. To explore this latter possibility, we assumed a first-order reaction with respect to particle concentration to solve for the inherent adsorption rate constant m_1 (equation (5), $n=1$) and then used the Arrhenius equation (Levine, 1988):

$$m_1 = A \cdot e^{(E_a/RT)} \tag{30}$$

to compare the natural log of the adsorption constant (m_1) with the inverse of temperature (T, in K). The activation energy (E_a) was calculated from the slope of this relation times R, the universal gas constant, 8.314 J mol^{-1} K^{-1}. The resulting values of E_a fall in the range of 50–90 kJ mol^{-1} for bottle- and MULVFS-based estimates of m_1'. These values compare favorably with the general range of values of E_a for reactions in aqueous solution (8–150 kJ mol^{-1}) (Levine, 1988). Such a correlation was not observed when this same analysis was performed with estimates of k_1' from the thorium sorption model. This analysis suggests that a dependence of the adsorption reaction on temperature could play an important role on influencing distributions with depth in the upper ocean.

The differences in the slopes suggest it is also possible that the coupled particle–^{234}Th model does not appropriately describe ^{234}Th cycling in the equatorial Pacific. This could occur in two ways: (1) ^{234}Th could be immediately re-adsorbed onto particles during remineralization, or (2) the particle pool could be composed of particles with different reactivity. Both of these scenarios have the effect that remineralization of particles does not affect particulate ^{234}Th. We do not have any means of confirming or refuting the first of these scenarios, the ^{234}Th cycle of which is equivalent to the simple sorption model. We explore the second of these scenarios in the next section.

Phytoplankton model. To simulate a particle pool composed of particles with different reactivity, we have developed the phytoplankton model described above in equations (13)–(18) and Fig. 3. We assume that phytoplankton compose 50% of the total particulate carbon concentration ($f=0.5$) based on the EqPac data sets of Barber *et al.* (1995) and Landry *et al.* (1995). This scenario doubles the rate constant of remineralization for the phytoplankton pool, P_{phy}. The refractory particles, P, have an infinite residence time with respect to remineralization (i.e. $\gamma=0$). The result of distinguishing between two types of particles effectively lowers m_1' to become more consistent with values of k_1' from the thorium sorption model (Fig. 11).

There are three lines of evidence that suggest that the phytoplankton model is more appropriate than the coupled particle–^{234}Th model for the central equatorial Pacific surface ocean. The first is that on average, only $48 \pm 11\%$ of the total biomass (Barber *et al.*, 1996, assuming C:Chl = 58; Kirchman *et al.*, 1995) was found to be composed of phytoplankton. The second line of evidence is that the average remineralization rate constant for the 0–100 m interval between 2°N and 2°S estimated from the bottle data ($\gamma=0.37\pm0.10$) is

approximately half the average phytoplankton growth rate ($\mu = 0.74 \pm 0.18$; Landry *et al.*, 1995) for this same latitude and depth region during Survey II. At steady state, γ and μ should be close to equal, as the sinking flux of particulate organic carbon has only a small contribution to the total flux balance (Murray *et al.*, 1996). These two pieces of evidence independently support the value of $f = 0.5$. The third line of evidence is that a relatively small amount of chlorophyll and relatively large amount of phaeopigments are caught in traps suggesting that direct aggregation and sinking is rare (J. Newton, personal communication). These three lines of evidence all suggest that the phytoplankton model better describes the fundamental processes behind particle and ^{234}Th cycling than the thorium sorption and couple particle–^{234}Th models.

Size-fractionated model

The size-fractionated model is a variation of the coupled particle–^{234}Th model, which distinguishes between small, suspended particles and large, sinking particles. Reversible, first-order aggregation couples the two particle pools which remineralize with the rate constant γ described earlier (equations 19–25). We use the comprehensive data set from the EqPac Survey cruises to calculate sinking rates and aggregation rate constants and compare our results with values calculated using this model at other sites.

Sinking rates of large particles. The size-fractionated model gives sinking rates, S_l, of the particles actually sinking as opposed to the total particle pool as calculated by the thorium sorption and simple coupled particle–^{234}Th models. It assumes that > 53 μm particles sink at a uniform velocity. Sinking rates were calculated from the advection-corrected sinking fluxes of ^{234}Th (F_{Th}), calculated from total ^{234}Th and the activity of ^{234}Th on large particles (Th_l) (equation 25). The sinking rates from the size-fractionated and thorium sorption models are compared in Fig. 13. Large particle sinking rates were 1–6 m day^{-1} in the upper

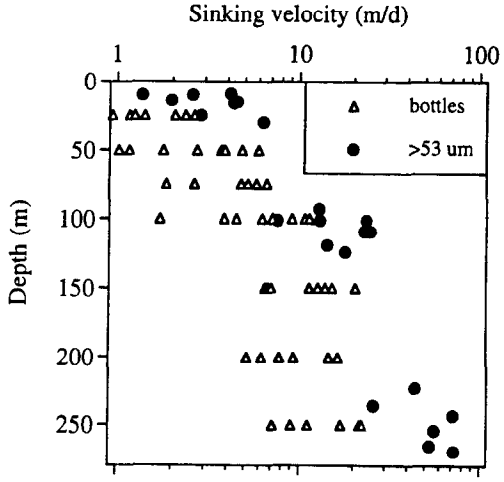

Fig. 13. Sinking velocities, (m day^{-1}) using the thorium sorption model (bottles) and the coupled particle–thorium model versus depth (m) for Survey II.

30 m and increased with depth to values of 26–72 m day^{-1} below 200 m. As discussed earlier, depth trends in S_l are due, in part, to the decrease in the activities of large particulate ^{234}Th with depth and, in part, due to maintenance of the radioactive deficiency between ^{234}Th and ^{238}U. Though this apparent increase in the sinking rate with depth may be a real feature in the equatorial Pacific, it is also likely that the large particle pool is differentiated in sinking velocity such that the fraction of suspended (as opposed to sinking) >53 μm material decreased with depth. This hypothesis is consistent with the observation of floating rhizoselenia mats at the front observed along 2°N (Archer *et al.*, 1997). No significant meridional trends were observed in large particle sinking rates. Sinking rates determined in a similar fashion by Bacon *et al.* (1996) during the JGOFS EqPac Time Series cruises are comparable with those of this work.

Aggregation and disaggregation. Much has been done to elucidate rates of aggregation and disaggregation using multiple thorium isotopes (Murnane *et al.*, 1990; Clegg *et al.*, 1991; Cochran *et al.*, 1993; Murnane *et al.*, 1994a,b, 1996). Clegg and Whitfield (1991) and Murnane *et al.* (1996) included remineralization in these calculations. Here we address the issue of aggregation and disaggregation in the context of the cycles of organic carbon and ^{234}Th. A convenient method of roughly gauging aggregation is to compare the C:^{234}Th ratio of small, suspended and large, sinking particles. The size-fractionated model predicts that large, sinking material will have a C:^{234}Th ratio that is greater than or equal to that of the small, suspended material; the only source of large particles is small particles and while remineralization rate constants are equal for large and small particulate carbon and ^{234}Th, only ^{234}Th has the additional loss term of radioactive decay. The timescale of aggregation and disaggregation can be gauged through the amount of excess ^{234}Th decay that has occurred in the large, sinking component. Mean and standard deviations for the C:^{234}Th ratio observed during EqPac Survey II in bottles, MULVFS 1–53 μm and MULVFS >53 μm are shown in Table 3 in three depth intervals. All three sample types showed a significant decrease in the C:^{234}Th ratio with depth ($P<0.05$ in each case). For comparison, drifting trap samples had a C:^{234}Th ratio of 3.6 ± 1.8 μmol dpm^{-1}. The data followed the order: (Bottles) > (traps) > (MULVFS >53 μm) > (MULVFS 1–53 μm) ($P<0.05$ in each case using the Mann–Whitney U-test). In general, the MULVFS data are consistent with the size-fractionated model. However, the C:^{234}Th ratios in MULVFS small and large particles are very similar such that individual calculations of the aggregation rate constant are swamped by the variability, spanning a range from negative to the infinite. The alternate assumption that bottle samples represent small particles and either MULVFS or the trap data represent large particles gives results inconsistent with the size fractionated model because the C:^{234}Th ratio decreases from small to large. These data suggest that either ^{234}Th

Table 3. *Summary of means and standard deviations for the organic carbon:^{234}Th ratio observed in bottles, MULVFS 1–53 μm and MULVFS > 53 μm material in the 0–50, 50–100 and 150–250 m depth ranges*

C/Th (μmol dpm^{-1})	0–50 m	54–101 m	109–269 m
Bottles	9.0 ± 4.1 ($n=26$)	6.1 ± 1.4 ($n=17$)	4.5 ± 1.5 ($n=25$)
MULVFS 1–53 μm	2.6 ± 1.1 ($n=19$)	1.4 ± 0.3 ($n=5$)	0.94 ± 0.27 ($n=23$)
MULVFS >53 μm	3.1 ± 1.2 ($n=8$)	1.7 ± 0.4 ($n=4$)	0.94 ± 0.28 ($n=10$)

is retained on particles during carbon remineralization or that the small, suspended particle pool is composed of two particle pools of differing C:^{234}Th ratio in which particles with the low C:^{234}Th ratio preferentially sink. This second hypothesis is consistent with the phytoplankton model. The C:^{234}Th ratio of MULVFS 1–53 μm particles is much lower than the C:^{234}Th ratio of trap material, consistent with the size fractionated model where aggregation is slow relative to other processes. This comparison gives a 90% confidence interval (using the Mann–Whitney U-test) for the aggregation rate constant in the upper 100 m of 0.0006–0.09 day^{-1} assuming a sinking rate, S_1, of 100 m day^{-1}. In summary, there is a severe inconsistency between sampling methods that prevents an unambiguous description of the size-fractionated model in the central equatorial Pacific. All aggregation scenarios are supported by some data comparisons, but none by all.

In order to compare aggregation for the EqPac surveys with other sites, we calculated aggregation rate constants by assuming a disaggregation rate constant of 5 day^{-1} from the Clegg and Whitfield (1993) model of the North Atlantic Bloom Experiment. Solving equation (19) for r_1 gives:

$$r_1 = \frac{(P_r - \gamma \cdot P_s + r_{-1} \cdot P_1)}{P_s} \tag{31}$$

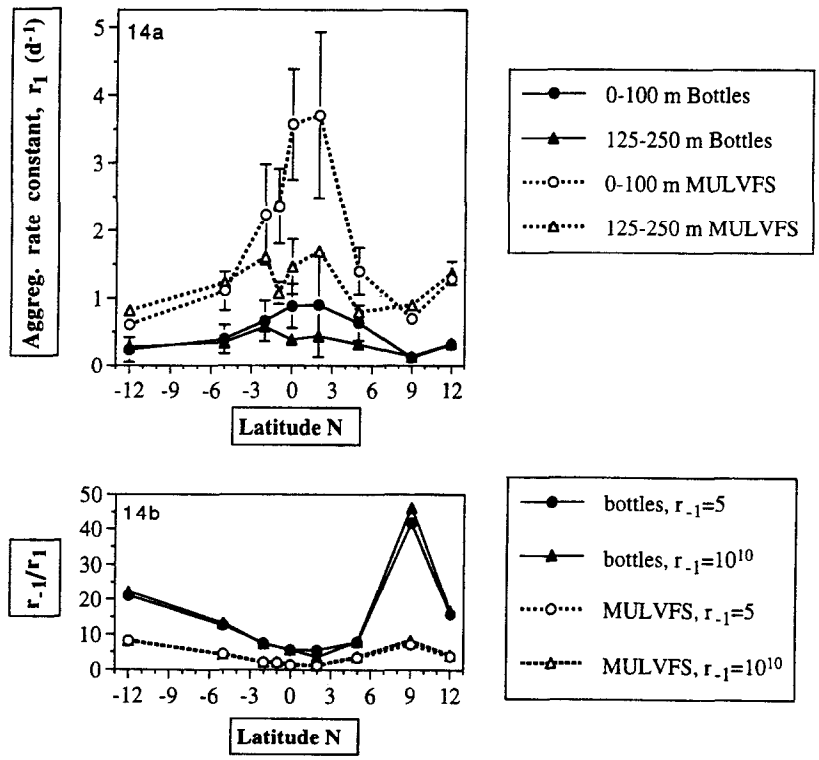

Fig. 14. (a) Average aggregation rate constants (day^{-1}) based on carbon from bottles and MULVFS data from the coupled particle–thorium model. Values are plotted for Survey II versus latitude for the 0–100 and 125–250 m depth ranges. (b) Average ratio of disaggregation to aggregation over the entire 0–100 m depth range assuming disaggregation rate constants of r_{-1} = 5 day^{-1} and 10^{10} day^{-1}.

Results for r_1 in the 0–100 m and 125–250 m depth ranges are shown in Fig. 14(a) for bottle and MULVFS estimates of γ and P_s. The values of r_1 from MULVFS were on average three to four times higher than bottles. In the upper 100 m, both estimates of r_1 had broad maxima centered slightly north of the equator at 3.7 day^{-1} for MULVFS and 0.9 day^{-1} for bottles. Values in the 0–100 m range decreased to values similar to the 125–250 m range (0.6–1.6 for MULVFS and 0.2–0.5 for bottles) off the equator.

The ratio of r_{-1}:r_1 is shown in Fig. 14(b). Included in Fig. 14(b) are values of the r_{-1}:r_1 ratio obtained as the disaggregation rate constant approaches infinity (r_{-1} set to 10^{10} day^{-1}). The similarity of these two values illustrates that an assumed value of $r_{-1} = 5$ day^{-1} corresponds to a disaggregation rate effectively infinite relative to the processes of remineralization and sinking implying that the model is insensitive to the value of r_{-1} at this magnitude. Results using these rate constants describe a scenario in which the C:^{234}Th is the same in small and large particles consistent with the small and large particle MULVFS data sets but not bottles or traps (Table 3).

Carbon and mass as indicators for particle cycle. ^{234}Th is generally considered to be a non-specific adsorber and thus a tracer for the cycling of particulate mass. As it is our goal to use ^{234}Th as a tracer of organic carbon, it is important to ascertain differences between the particle cycling of mass and organic carbon. Most previous modeling studies (for example, Clegg and Whitfield, 1990, 1991; Clegg *et al.*, 1991; Murnane *et al.*, 1990) described particle cycles on a mass basis. Murnane *et al.* (1996) included cycling of particulate organic carbon and mass to estimate remineralization and aggregation rate constants, respectively, but did not directly compare the two cycles. Here we provide circumstantial evidence that organic carbon tracked mass during EqPac. Depth and meridional variations were observed in the organic carbon to mass ratio in the upper 250 m in the EqPac Survey II data set. In the upper 100 m MULVFS 1–53 μm particles were $33 \pm 5\%$ organic carbon which is close to the Redfield value of 37% for soft tissues ($(CH_2O)_{105}N_{15}P$; Broeker and Peng, 1982). This implies that particles in the upper 100 m were composed of approximately 89% organic matter. Particles in the 100–269 m depth range contained a much lower value of $20 \pm 5\%$ organic carbon, suggesting either preferential remineralization of organic material or preferential sinking of inorganic material or both. There was a statistically significant decrease in organic carbon content with depth at a given location in the small particulate material but not in trap samples or the MULVFS > 53 μm fractions. We also observed a significant decrease in the organic carbon to mass ratio towards the equator in both trap and MULVFS > 53 μm samples but not in the MULVFS 1–53 μm samples. The correlation of beam attenuation with MULVFS organic carbon ($r^2 = 0.96$) was stronger than the correlation with MULVFS mass ($r^2 = 0.82$) (Bishop, in press), suggesting that beam attenuation data can be calibrated and used as a proxy for either total particulate mass or carbon. We conclude that organic carbon and total mass track each other quite well in the upper 100 m off the equator, but less well below the euphotic zone and at the equator. As thorium adsorption is thought to track mass not organic carbon, organic carbon-based remineralization rate constants may be overestimates in these zones, as thorium and organic carbon cycling may be less coupled.

Average values for the remineralization rate constant (γ), adsorption rate constant (m_1'), aggregation rate constant (r_1) and sinking velocity (S_1) using particulate concentrations from MULVFS mass, bottle organic carbon and MULVFS organic carbon data are shown in Fig. 15 for Survey I and Survey II in equatorial (2°N–2°S) and off-equatorial (12°–3°N,S)

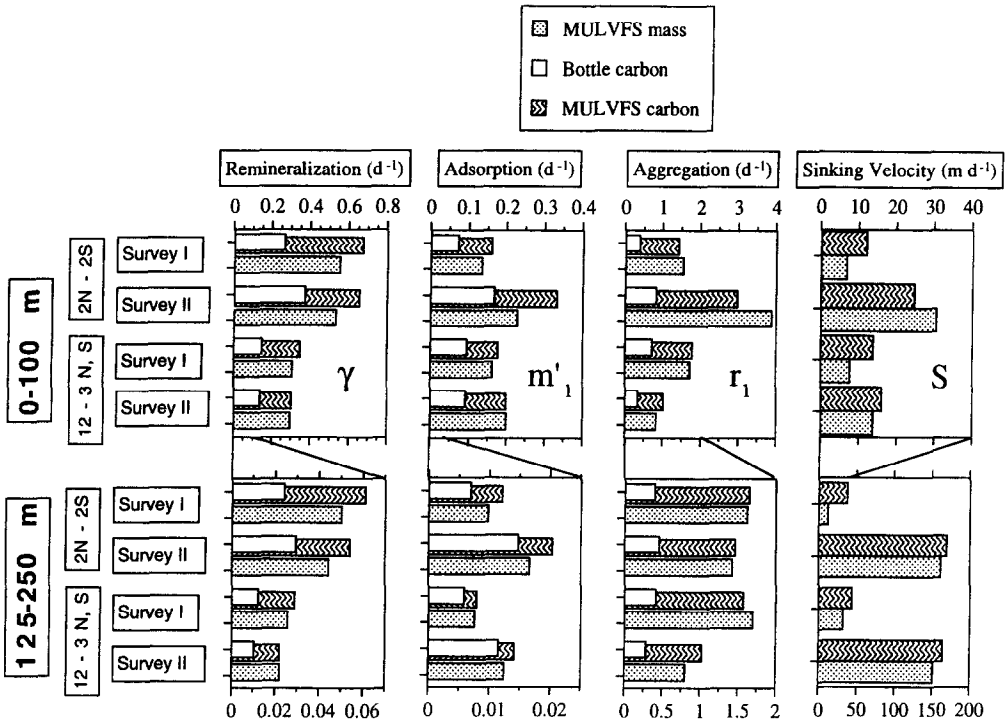

Fig. 15. Bar summary of average remineralization, adsorption and aggregation rate constants (day^{-1}) determined for the EqPac Survey cruises grouped by Survey (I and II), latitude band (2°N–2°S and 12°–3° N,S), depth range (0–100 m and 125–250 m) and data type (MULVFS mass, bottle carbon and MULVFS carbon).

bins. Estimates of these rate constants based on organic carbon and total mass from MULVFS were generally indistinguishable-estimates of γ from organic carbon averaged only 12% higher than estimates from mass. Again, a much larger difference was seen between bottle and MULVFS estimates, where bottle estimates of γ averaged 53% lower than estimates from MULVFS. Results for Survey I were quite similar to those from Survey II, on which we have concentrated our discussion. Estimates of γ from the equatorial bin were higher than from the off-equatorial bin during both Survey I and Survey II.

One large difference between Survey I and Survey II was in the observed sinking velocities. During Survey I, sinking rates increased only modestly with depth. During Survey II, there were significant increases in sinking velocities with depth both on and off the equator. The sinking velocities of mass and carbon for Survey II are significantly higher than sinking velocities of ^{234}Th shown in Fig. 13. This is because the trap material used to convert the ^{234}Th flux to a mass or carbon flux and the MULVFS > 53 μm material used for the large particle concentration have different C:^{234}Th ratios.

Comparison with other sites. Average rate constants for adsorption, remineralization, and aggregation for the 0–100 m and 125–250 m depth ranges of both EqPac Survey Cruises are shown in Fig. 16 along with previously published results for Vertex 4, Panama Basin and NABE studies (Clegg and Whitfield, 1991, 1993; Clegg *et al.*, 1991). Remineralization rate

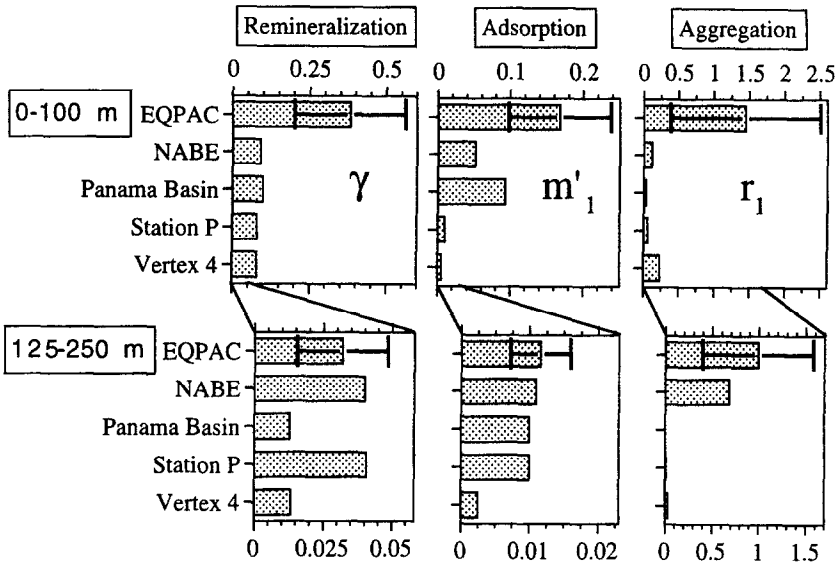

Fig. 16. Bar summary of average remineralization, adsorption and aggregation rate constants (day^{-1}) determined for the EqPac Survey cruises compared to sites studied by Clegg and Whitfield (1991a,b, 1993).

constants, γ, were calculated by us from primary production, particle concentration and flux data, except for station P where γ was calculated from multiple thorium isotopes (Clegg *et al.*, 1991). In the 125–250 m depth range, estimates of remineralization and adsorption rate constants converge to similar, low values. Average EqPac estimates for all three of these rate parameters in the 0–100 m depth range were, in general, higher than any previously seen except for the Clegg and Whitfield (1993) analysis of the Panama Basin data set of Murray *et al.* (1989), which gave estimates of m_1' comparable with the bottle estimate of adsorption during EqPac.

Estimates of aggregation rate constant (r_1) in the upper 100 m during EqPac were much higher than all previous studies. Aggregation rate constant estimates in the 125–250 m depth range were much higher than all but the NABE site, which, like our study, assumed a relatively high disaggregation rate constant of $r_{-1} = 5\ day^{-1}$. Estimates of the aggregation rate constant, r_1, are much greater than previous studies because the measured values of large particle concentrations from MULVFS > 53 μm data are an order of magnitude larger than those estimated using the method of Clegg and Whitfield (1991, 1993) who were forced to infer P_1 from a flux estimate and a sinking rate between 100–150 m day^{-1}. The measured ratio of large to small particles (P_l/P_s) from MULVFS organic carbon data taken during Survey II in the upper 100 m was 0.41 ± 0.27.

High values of m_1' (equation (29)) in EqPac are partially a result of differences in the magnitude of the ^{234}Th deficiency. Over the month-long NABE, the dissolved ^{234}Th activity decreased dramatically, and, as a result, the ^{234}Th deficiency increased by a factor of 4 over the course of the study (Buesseler *et al.*, 1992). The Vertex 4 site had a negligible ^{234}Th deficiency, giving low values of m_1'. In the Panama Basin, ^{234}Th deficiencies resembled those observed during EqPac.

Table 4. Summary of averaged data on integrated primary production ($\int P_r$, mmol C m^{-2} day^{-1}), integrated particle load ($\int P$, mmol C m^{-2}) in the upper 100 m, the sinking particle flux past 100 m (F, mmol C m^{-2} day^{-1}) from previously published work and the resulting value of γ

Site	$\int P_r$ (mmol C m^{-2} day^{-1})	$\int P$ (mmol C m^{-2})	F (mmol C m^{-2} day^{-1})	γ (day^{-1})	Source
Oligotrophic					
VERTEX IV	33	244	2	0.13	Coale and Bruland, 1987; Knauer *et al.*, 1984
BATS	30	233	2	0.12	Michaels *et al.*, 1994; Knap *et al.*, 1994
HOT	34	207	2	0.15	Karl *et al.*, 1995; Winn *et al.*, 1993
Subsurface nitrate					
VERTEX II	63	373	3	0.16	Coale and Bruland, 1987; Knauer *et al.*, 1984
Panama Basin	31	350	7	0.07	Murray *et al.*, 1989
EqPac-I 12°–3°	39	213	3	0.17	Murray *et al.*, 1996
EqPac-II 12°–3°	38	232	6	0.14	Murray *et al.*, 1996
Surface nitrate					
MLML P.C.-2	57	452	15	0.09	Coale and Bruland, 1985
Stn. P (Super)	59	707	6	0.08	Welschmeyer *et al.*, 1993; Wheeler, 1993
NABE	101	668	24	0.11	Lochte *et al.*, 1993; Buesseler *et al.*, 1992
EqPac-I 2°–2°	63	222	3	0.27	Murray *et al.*, 1996
EqPac-II 2°–2°	116	285	10	0.37	Murray *et al.*, 1996

Note: Wheeler (1993) estimates of ^{15}N production at Station P are used for F and PON as particle concentration (both converted to carbon using the mole ratio of 6.6 of Broecker and Peng, 1982). All other estimates of F are directly from sediment traps, except for the Panama Basin, EqPac and NABE estimates which are ^{234}Th-corrected. The nearest available estimate of the sinking flux of particulate organic carbon at 100 m is used directly (e.g. MLML P.C.-2 at 65 m and BATS, HOT, NABE at 150 m).

An important factor for EqPac was that the high values of γ resulted in high values of m_1' relative to other sites. Average values of integrated primary production ($\int P_r$), integrated particle load from bottles ($\int P$) and sinking flux (F) in the upper 100 m are shown in Table 4 for three oligotrophic sites: VERTEX IV (~900 km north of Oahu, HI; Knauer *et al.*, 1984; Coale and Bruland, 1987), BATS (~50 km south of Bermuda; Michaels *et al.*, 1994; Knap *et al.*, 1994), HOT (~100 km north of Oahu, HI; Winn *et al.*, 1993; Karl *et al.*, 1995), four study sites with consistently present sub-surface nitrate: VERTEX II (300 km SW of central Mexico; Knauer *et al.*, 1984; Coale and Bruland, 1987), Panama Basin (Murray *et al.*, 1989), EqPac I 2°–2°(Murray *et al.*, 1996) and EqPac II 12°–3°(Murray *et al.*, 1996), as well as five eutrophic study sites with consistently present surface nitrate: the Moss Landing Marine Labs PIT cruise 2 (~100 km west of Santa Cruz, CA; Coale and Bruland, 1985), Station P (the SUPER program-50°N, 145°W; Welschmeyer *et al.*, 1993; Wheeler, 1993), NABE (47°N, 20°W; Buesseler *et al.*, 1992; Lochte *et al.*, 1993), EqPac I 12°–3°(Murray *et al.*, 1996) and EqPac II 2°–2°(Murray *et al.*, 1996). We also show the resulting remineralization rate constant (γ) calculated from these data. The three oligotrophic sites had low and very consistent values of integrated primary production, integrated particle load and sinking flux. Combined with the sites with consistent subsurface nitrate gives a remarkably constant value of $\gamma = 0.13 \pm 0.03$ day^{-1} in the upper 100 m. The eutrophic sites can be divided into two categories: coastal and high latitude sites with high particle concentration and lower γ (e.g. MLML P.C. 2; Stn P;

NABE) versus equatorial sites (e.g. EqPac Survey I and Survey II) with low particle concentration and higher γ. Comparison of the central equatorial Pacific with other sites emphasizes the relatively intense biological cycling between 2°N and 2°S. In the presence of macronutrients and abundant solar irradiance and absence of atmospheric inputs, specific growth rates of small phytoplankton are large (Coale *et al.*, 1996; Landry *et al.*, 1997). In the absence of allochthonous fluxes from wind or sediment transport, the result is a nutrient-rich euphotic zone dominated by a rapidly recycling microbial loop from which it is rare that particles escape (Murray *et al.*, 1996).

SUMMARY AND CONCLUSIONS

Dissolved and particulate ^{234}Th data taken during the US JGOFS-EqPac Survey cruises from 12°N to 12°S along 140°W were used to evaluate ^{234}Th and particle cycling in the central equatorial Pacific. Rate constants of ^{234}Th and particle cycling were derived using a sequence of particle and ^{234}Th cycling models of increasing complexity. We found that sampling methodology, MULVFS versus bottle, had a large impact on model results and recommend further efforts towards understanding the causes of these differences. Particulate organic carbon and ^{234}Th data sets collected by in-situ pump (MULVFS) and bottle approaches were carried through in parallel calculations.

Using the thorium sorption model, we observed a strong seasonal difference in the latitudinal trend of adsorption rate constants, k_1'. Values of k_1' ranged from 0.02 to 0.04 day^{-1} in the upper 75 m to 0.01 day^{-1} below 200 m. Sinking rates for the total particle pool ranged from 1 to 7 m day^{-1} at 0–75 m to 10 to 23 m day^{-1} below 200 m. There was a good correlation between k_1' and particle concentration. These results were consistent with other studies at similar particle concentrations. The relationship between k_1' and particle concentration suggested that the effect of particle concentration on thorium adsorption rate constants may reach a plateau value at particle concentrations greater than 300 mg m^{-3}.

Results from the coupled particle–^{234}Th model suggested that the central equatorial Pacific had more rapid particle recycling than any other region previously studied using this model. Though the absolute value of ^{234}Th recycling remains uncertain due to different results using bottle and MULVFS sampling techniques, values of the remineralization rate constant, γ, were at least 0.3 day^{-1} in the upper 0–100 m from 2°N to 2°S during Survey II. Values of γ at higher latitudes than 2°N, S were roughly half these values. The values of the adsorption rate constant, m_1', derived from the coupled particle–^{234}Th model were two to six times higher than those from the thorium sorption model and had a very strong correlation with particle concentration and depth. Future studies should test the temperature effect on ^{234}Th adsorption.

A second coupled model, the phytoplankton model, was introduced to distinguish between rapidly-recycling phytoplankton and more refractory pools of carbon. Our results suggested that the coupled particle–^{234}Th model over-estimates adsorption rates. We suggest that the phytoplankton model is a more appropriate model for this region. This is because the particles which remineralize do not have long enough residence times to adsorb significant amounts of ^{234}Th. As a result, remineralization and adsorption are effectively decoupled.

Our results from a third coupled model, size-fractionated model, showed that unique aggregation scenarios are difficult to determine because of the conflicting data sets from

sediment trap, MULVFS and bottle sampling approaches. Large particle sinking rates, S_1, were quite low in the upper 30 m with values of 1–6 m day^{-1} and increased dramatically with depth to values of 26–72 m day^{-1} below 200 m. High ^{234}Th activities in the > 53 μm MULVFS fraction resulted in lower sinking rates and lower values of the aggregation to disaggregation ratio than those found by Clegg and Whitfield (1991, 1993) and Clegg *et al.* (1991). However, large particles (> 53 μm MULVFS) and particles caught in sediment traps were found to have significantly different organic carbon to ^{234}Th ratios.

From this study we conclude the following.

(1) Scavenging (net adsorption of ^{234}Th and removal of particles by sinking) is faster in the central equatorial Pacific than in the oligotrophic Pacific (Bruland and Coale, 1986), but slower than in coastal and shelf mesotrophic regions (Coale and Bruland, 1985, 1987). Adsorption rate constants (k_1') increase with increasing particle concentrations up to about 300 mg m^{-3} and then remain constant. This result is in contrast to the results of Honeyman *et al.* (1988).

(2) Recycling of particulate organic carbon in the euphotic zone of the central equatorial Pacific was two to ten times greater than sites previously studied. This is due to the relative importance of remineralization in the food web of the equatorial Pacific illustrating the dominance and efficiency of the microbial loop, wherein microzooplankton grazing nearly balance the high specific rates of primary production by small cells (Frost and Franzen, 1992; Murray *et al.*, 1995; Landry *et al.*, 1997). As a consequence of this, organic matter cycling dominates mass cycling in the upper 100 m, and ^{234}Th cycling traces mass and carbon almost equally.

(3) Adsorption rate constants from the thorium sorption, coupled particle–^{234}Th and phytoplankton models were extremely sensitive to the model-treatment of remineralization. Net adsorption from the thorium sorption model (k_1') was only a small fraction of total adsorption from the coupled particle–^{234}Th model (m_1'). The coupled particle–^{234}Th model, assuming a homogeneously recycling particle pool, suggested that ^{234}Th recycles three to four times between the dissolved and particulate phases before being removed on particles. As values of k_1' do not reflect total adsorption but are the result of the competing processes of adsorption and remineralization, comparisons of k_1' between sites made here and in the literature may be inappropriate and should be re-evaluated.

(4) The phytoplankton model, assuming that particle cycling is differential with respect to remineralization, suggested that the adsorption was grossly over-estimated by the coupled particle–^{234}Th model and under-estimated by the simple sorption model. This model should be investigated further in future studies.

Considering the dominance of the microbial loop on the particle cycle and the variability of the C:^{234}Th ratio, we suggest that the particle removal depends on a mechanism of differential remineralization of particles in the euphotic zone and sinking of relatively refractory particles. As the C:^{234}Th ratio in sinking particles is a crucial measurement for ^{234}Th estimates of the sinking flux of organic carbon, future work should address causes for variability in this ratio and specifically attempt to identify when > 53 μm material can be considered representative of sinking material.

Acknowledgements—We thank Barbara Paul for help with sample collection and analysis, Thomas Chapin for whole bottle filtration, Lewis Lu for particulate organic carbon analysis and Steve Emerson, Burke Hales, Bruce Frost and two anonymous reviewers for useful criticism and suggestions. This research was supported by NSF

grant # 9022466 and NASA Global Change (Earth System Science) Fellowship # 1995-GlobalCh00307, School of Oceanography Contribution Number 2183, and US JGOFS Contribution Number 387. Musical Inspiration by Diamond Fist Werny.

REFERENCES

Altabet, M. A., Bishop, J. and Mccarthy, J. (1992) Differences in particulate nitrogen concentration and isotopic composition for samples collected by bottles and large-volume pumps in Gulf Stream warm core rings and the Sargasso Sea. *Deep-Sea Research*, **39**, S405–S417.

Archer, D. (1997) A meeting place of great ocean currents: shipboard observations of a convergent front at 2°N in the Pacific. *Deep-Sea Research II*, **44**, 1827–1849.

Balistrieri, L., Brewer, P.G. and Murray, J.W. (1981) Scavenging residence times of trace metals and surface chemistry of sinking particles in the deep ocean. *Deep-Sea Research*, **28**(2A), 101–121.

Bacon, M.P. and Anderson, R.F. (1982) Distributions of thorium isotopes between dissolved and particulate forms in the deep sea. *Journal of Geophysical Research*, **87**(C3), 2045–2056.

Bacon, M. P., Cochran, J. K., Hirshberg, D., Hammar, T. R. and Fleer, A. P. (1996) Export fluxes of carbon at the equator during the EqPac time-series cruises estimated from ^{234}Th measurements. *Deep-Sea Research II*, **43**, 1133–1154.

Barber, R. T., Sanderson, M. P., Lindley, S. T., Chai, F., Newton, J., Trees, C. C., Foley, D. G. and Chavez, F. P. (1996) Primary production in the equatorial Pacific along 140°W. *Deep-Sea Research II*, **43**, 933–970.

Baskaran, M., Sanschi, P. H., Benoit, G. and Honeyman, B. D. (1992) Scavenging of thorium isotopes by colloids in seawater of the Gulf of Mexico. *Geochimica et Cosmochimica Acta*, **56**, 3375–3388.

Bishop, J. K.B. and Edmond, J. M. (1976) A new large-volume filtration system for the sampling of oceanic particulate matter. *Journal of Marine Research*, **34**, 181–198.

Bishop, J. K.B., Schpack, D., Sherrel, R. M. and Conte, M. (1985) A multiple-unit large-volume filtration system for sampling oceanic particulate matter in mesoscale environments. In *Mapping Strategies in Chemical Oceanography*, ed. A. Zirino, Advances in Chemistry Series No. 209. pp. 155–175. The American Chemical Society,

Bishop, J. K. B. (in press) Particulate organic carbon/particulate dry weight and beam attenuation coefficient measurements. *Deep-Sea Research I*, in press.

Broecker, W. S. and Peng, T-H., (1982) *Tracers in the Sea*, 690 pp. Lamont-Doherty Geological Observatory, Columbia University, NY.

Buesseler, K. O., Bacon, M., Cochran, J. K. and Livingston, H. (1992) Carbon and nitrogen export during the JGOFS North Atlantic Bloom Experiment estimated from ^{234}Th:^{238}U disequilibria. *Deep-Sea Research*, **39**, 1115–1137.

Buesseler, K. O., Andrews, J., Hartman, M., Belastock, R. and Chai, F. (1995) Regional estimates of the export flux of particulate organic carbon derived from thorium-^{234} during the JGOFS EqPac program. *Deep-Sea Research II*, **42**, 777–804.

Bruland, K. W., and Coale, K. H. (1986) Surface water ^{234}Th/^{238}U disequilibria: spatial and temporal variations of scavenging rates within the Pacific Ocean. In *Dynamic Processes in the Chemistry of the Upper Ocean*, ed. J. D. Burton, P. J. Brewer and R. Chesselet, pp. 159–172. Plenum, New York.

Chai, F. (1995) Origin and maintainance of high nitrate condition in the equatorial Pacific, a biological–physical model study. Ph. D. dissertation, Duke University, Durham, NC, 170 pp.

Chen, J. H., Edwards, R. L. and Wasserburg, G. J. (1986) ^{238}U, ^{234}U and ^{232}Th in seawater. *Earth and Planetary Science Letters*, **80**, 241–251.

Chung, S. P., Gardner, W. D., Richardson, M. J. and Walsh, I. D. (1996) Beam attenuation and microorganisms: spatial and temporal variations in small particles along 140°W during the 1992 JGOFS-EqPac transects. *Deep-Sea Research II*, **43**, 1205–1226.

Clegg, S. L. and Whitfield, M. (1990) A generalized model for the scavenging of trace metals in the open ocean—I Particle cycling. *Deep-Sea Research*, **37**, 809–832.

Clegg, S. L. and Whitfield, M. (1991) A generalized model for the scavenging of trace metals in the open ocean—I Thorium scavenging. *Deep-Sea Research*, **38**, 91–120.

Clegg, S.L., Bacon, M.P. and Whitfield, M. (1991) Application of a generalized scavenging model to thorium isotope and particle data at equatorial and high-latitude sites in the Pacific ocean. *Journal of Geophysical Research*, **96**, 20655–20670.

Clegg, S. L. and Whitfield, M. (1993) Application of a generalized scavenging model to time series ^{234}Th and particle data obtained during the JGOFS North Atlantic Bloom Experiment. *Deep-Sea Research*, **40**, 1529–1545.

Coale, K. H. and Bruland, K. W. (1985) ^{234}Th:^{238}U disequilibria within the California Current. *Limnology and Oceanography*, **30**, 22–33.

Coale, K. H. and Bruland, K. W. (1987) Oceanic stratified euphotic zone as elucidated by ^{234}Th:^{234}U disequilibria. *Limnology and Oceanography*, **32**, 198–200.

Coale, K. H., Fitzwater, S. E., Gordon, R. M., Johnson, K. S. and Barber, R. T. (1996) Control of community growth and export production by upwelled iron in the equatorial Pacific ocean. *Nature*, **379**, 621–624.

Cochran, J. K., Carey, A. E., Sholkovitz, E. A. and Suprenant, L. D. (1986) The geochemistry of uranium and thorium in coastal marine sediments and sediment pore waters. *Geochimica et Cosmochimica Acta*, **50**, 663–680.

Cochran, J. K., Buesseler, K. O., Bacon, M. P. and Livingston, H. D. (1993) Thorium isotopes as indicators of particle dynamics in the upper ocean: results from the JGOFS North Atlantic Bloom Experiment. *Deep-Sea Research I*, **40**, 1569–1595.

Diercks, A. R. and Asper, V. L. (1997) *In situ* settling speeds of marine snow aggregates below the mixed layer: Black Sea and Gulf of Mexico. *Deep-Sea Research I*, **40**, 1569–1595.

Dunne, J. P., and Murray, J. W. (submitted) Two dimensional simulations of ^{234}Th distributions and export flux in the central equatorial Pacific. *Deep-Sea Research.*

Duce, R. A. and Tindale, R. A. (1991) Atmospheric transport of iron and its deposition in the ocean. *Limnology and Oceanography*, **36**, 1715–1726.

Emerson, S. (1987) Seasonal oxygen cycles and biological new production in surface waters of the subarctic Pacific Ocean. *Journal of Geophysical Research*, **92**, 6535–6544.

Frost, B. W. and Franzen, N. C. (1992) Grazing and iron limitation in the control of phytoplankton stock and nutrient concentration: a chemostat analogue of the Pacific equatorial upwelling zone. *Marine Ecology Progress Series*, **83**, 291–303.

Honeyman, B. D., Balestrieri, L. S. and Murray, J. W. (1988) Oceanic trace metal scavenging: the importance of particle concentration. *Deep-Sea Research*, **35**, 227–246.

Honeyman, B. D. and Santschi, P. H. (1989) A Brownian-pumping model for oceanic trace metal scavenging: evidence from Th isotopes. *Journal of Marine Research*, **47**, 951–992.

Honjo, S., Dymond, J., Collier, R. and Manganini, S. J. (1995) Export production of particles to the interior of the equatorial Pacific Ocean during the 1992 EqPac experiment. *Deep-Sea Research II*, **42**, 831–870.

Jenkins, W. J. (1987) ^{3}H and ^{3}He in the Beta Triangle: observations of Gyre ventilation and oxygen utilization rates. *Journal of Physical Oceanography*, **17**, 763–783.

Karl, D. M., Christian, J. R., Dore, J. E., Hebel, D. V., Letelier, R. M., Tupas, L. M. and Winn, C. D. (1996) Seasonal and interannual variability in primary production and particle flux at station ALOHA. *Deep-Sea Research II*, **43**, 539–568.

Kessler, W. S. and McPhaden, M. J. (1995) The 1991–1993 El Niño in the central Pacific. *Deep-Sea Research II*, **42**, 295–334.

Kirchman, D. L., Rich, J. H. and Barber, R. T. (1995) Biomass and biomass production of heterotrophic bacteria along 140°W in the equatorial Pacific: effect of temperature on the microbial loop. *Deep-Sea Research II*, **42**, 603–620.

Knap, A. H., Michaels, A. F., Dow, R. L., Johnson, R. J., Gundersen, K., Sorensen, J. C., Close, A. R., Howse, F. A., Bates, N., Best, M., Hammer, M. and Doyle A. P. (1994) *Data Report for BATS 37-BATS 48, October, 1991–September, 1992.* Bermuda Biological Station for Research, Inc.

Knauer, G. A., Martin, J. H. and Karl, D. M. (1984) The flux of particulate organic matter out of the euphotic zone, *Workshop on the Global Ocean Flux Study*, Woods Hole, MA.

Ku, T.-L., Knauss, K. G. and Mathieu, G. G. (1977) Uranium in open ocean: concentration and isotopic composition. *Deep-Sea Research*, **24**, 1005–1017.

Landry, M. R., Constantinou, J. and Kirshtein, J. (1995) Microzooplankton grazing in the central equatorial Pacific during February and August, 1992. *Deep-Sea Research II*, **42**, 657–672.

Landry, M. R., Barber, R. T., Bidigare, R. R., Chai, F., Coale, K., Dam, H. G., Lewis, M. R., Lindley, S. T., Mccarthy, J. J., Roman, M. R., Verity, P. G. and White, J. (1997) Iron and grazing constraints on primary production in the central equatorial Pacific: an EqPac synthesis. *Limnology and Oceanography*, **42**, 405–418.

Laws, E. A. (1991) Photosynthetic quotients, new production and net community production in the open ocean. *Deep-Sea Research I*, **38**, 143–167.

Levine, I. A. (1988) *Physical Chemistry*, 3rd edn., p. 561. McGraw-Hill, New York.

Liang, Y., Murray, J. W., Balistrieri, L. S. and Paul, B. (submitted) Evaluation of the Brownian-Pumping model: colloidal ^{234}Th in Puget Sound, WA. *Journal of Marine Research.*

Lochte, H. W., Ducklow, H. W., Fasham, M. J.R. and Steinen, C. (1993) Plankton succession and carbon cycling at 47°N 20°W during the JGOFS North Atlantic Bloom Experiment. *Deep-Sea Research II*, **40**, 91–114.

Martin, J. H., Knauer, G. A., Karl, D. M. and Broenkow, W. W. (1987) VERTEX: carbon cycling in the northeast Pacific. *Deep-Sea Research*, **34**, 267–285.

Michaels, A. F., Bates, N. R., Buesseler, K. O., Carlson, C. A. and Knap, A. H. (1994) Carbon-cycle imbalances in the Sargasso Sea. *Nature*, **372**, 537–540.

Moran, S. B. and Buesseler, K. O. (1993) Size-fractionated ^{234}Th in continantal shelf waters off New England: implications for the role of colloids in oceanic trace metal scavenging. *Journal of Marine Research*, **51**, 893–922.

Murnane, R.J., Sarmiento, J.L. and Bacon, M. (1990) Thorium isotopes, particle cycling models, and inverse calculations of model rate constants. *Journal of Geophysical Research*, **95**, 16195–16206.

Murnane, R. J., Cochran, J. K. and Sarmiento, J. L. (1994) Estimates of particle- and thorium-cycling rates in the northwest Atlantic Ocean. *Journal of Geophysical Research*, **99**(c2), 3373–3392.

Murnane, R. J., Cochran, J. K. and Sarmiento, J. L. (1994) Determination of thorium and particulate matter cycling parameters at station P: a reanalysis and comparison of least squares techniques. *Journal of Geophysical Research*, **99**(c2), 3393–3405.

Murnane, R. J., Cochran, J. K., Buesseler, K. O. and Bacon, M. P. (1996) Least-squares estimates of thorium, particle and nutrient cycling rate constants from the JGOFS North Atlantic Bloom Experiment. *Deep-Sea Research I*, **43**, 239–258.

Murray, J. W., Downs, J. N., Strom, S., Wei, C.-L. and Jannasch, H. W. (1989) Nutrient assimilation, export production and ^{234}Th scavenging in the eastern equatorial Pacific. *Deep-Sea Research*, **36**, 1471–1489.

Murray, J. W., Barber, R. T., Roman, M. R., Bacon, M. P. and Feely, R. A. (1994) Physical and biological controls on carbon cycling in the equatorial Pacific. *Science*, **266**, 58–65.

Murray, J. W., Johnson, E. and Garside, C. (1995) AU.S. JGOFS Process Study in the equatorial Pacific (EqPac): introduction. *Deep-Sea Research II*, **42**, 275–294.

Murray, J. W., Young, J., Newton, J., Dunne, J. P., Chapin, T. and Paul, B. (1996) Export production determined using ^{234}Th:^{2238}U disequilibria. *Deep-Sea Research II*, **43**, 1095–1132.

Najjar, R. G., Sarmiento, J. L. and Toggweiler, J. R. (1992) Downward transport and fate of organic matter in the ocean: simulations with a general circulation model. *Global Biogeochemical Cycles*, **6**, 45–76.

Niven, S. E.H., Kepkay, P. E. and Boraie, A. (1995) Colloidal organic carbon and colloidal ^{234}Th dynamics during a coastal phytoplankton bloom. *Deep-Sea Research II*, **42**, 257–273.

Pace, M. L., Knauer, G. A., Karl, D. M. and Martin, J. H. (1987) Primary production, new production and vertical flux in the eastern Pacific Ocean. *Nature*, **325**, 803–804.

Quigley, M. S., Honeyman, B. D. and Santschi, P. H. (1996) Thorium sorption in the marine environment: equilibrium partitioning at the hematite/water interface, sorption/desorption kinetics an particle tracing. *Aquatic Geochemistry*, **1**, 277–301.

Rohlf, F. J. and Sokal, R. R. (1995) *Statistical Tables*, 3rd edn. W. H. Freeman and Co., New York, NY.

Sokal, R. R. and Rohlf, F. J. (1995) *Biometry*, 3rd edn. W. H. Freeman and Co., New York, NY.

Tupas, L., Santiago-Mandujano, F., Hebel, D., Firing, E., Lukas, R. and Karl, D. (1995) Hawaii Ocean Time-series Data Report 6: 1994, University of Hawaii.

Walsh, I. D., Chung, S. P., Richardson, M. J. and Gardner, W. D. (1995) The diel cycle in the integrated particle load in the equatorial Pacific: a comparison with primary production. *Deep-Sea Research*, **42**, 465–478.

Wei, C.-L. and Murray, J. W. (1992) Temporal variations of ^{234}Th activity in the water column of Dabob Bay: particle scavenging. *Limnology and Oceanography*, **37**(2), 297–314.

Wei, C.-L. and Murray, J. W. (1991) ^{234}Th/^{238}U disequilibria in the Black Sea. *Deep-Sea Research*, **38**(2A), S855–S874.

Welschmeyer, N. A., Strom, S., Goericke, R., Ditullio, G., Belvin, M. and Peterson, W. (1993) Primary production in the subarctic Pacific Ocean: Project SUPER. *Progress in Oceanography*, **32**, 101–136.

Wheeler, P. A. (1993) New production in the subarctic Pacific Ocean: net changes in nitrate concentrations, rates of nitrate assimilation and accumulation of particulate nitrogen. *Progress in Oceanography*, **32**, 137–162.

Winn, C., Lukas, R., Karl, D. and Firing, E. (1993) Hawaii Ocean Time-series Data Report 3: 1991, University of Hawaii.

Williams, P. J.Leb. and Purdie, D. A. (1991) In vitro and in situ derived rates of gross production, net community production and respiration of oxygen in the oligotrophic subtropical gyre of the North Pacific Ocean. *Deep-Sea Research I*, **38**, 891–910.

Williams, P. J.Leb. and Robertson, J. E. (1991) Overall planktonic oxygen and carbon dioxide metabolisms: the problem of reconciling observations and calculations of photosynthetic quotients. *J. Plankton Research*, **13**, 153–169.